A data-driven digital-twin model and control of high temperature proton exchange membrane electrolyzer cells

Dongqi Zhao[a], Qijiao He[b], Jie Yu[b], Meiting Guo[b], Jun Fu[a], Xi Li[a]*, Meng Ni[b]*

a. School of Artificial Intelligence and Automation, Key Laboratory of Image Processing and Intelligent Control of Education Ministry, Huazhong University of Science and Technology, Wuhan, Hubei, China.

b. Department of Building and Real Estate, Research Institute for Sustainable Urban Development (RISUD) and Research Institute for Smart Energy (RISE), The Hong Kong Polytechnic University, Hung Hom, Kowloon, Hong Kong.

*Corresponding author: Xi Li and Meng Ni.

E-mail address: lixi_wh@126.com (Xi Li), meng.ni@polyu.edu.hk (Meng Ni).

Abstract

The high temperature proton exchange membrane electrolyzer cells (HT-PEMEC) is promising for hydrogen generation from fluctuating and intermittent renewable energy. In this study, a data-driven method is developed to study the dynamic behavior of HT-PEMEC. This method combines multiphysics simulation and nonlinear system identification, avoiding expensive experimental costs and time-consuming full multiphysics calculations. Dynamic models for predicting the power consumption, hydrogen production and temperature are identified, and show high accuracy compared with multiphysics models. Subsequently, the identification model was used to predict the dynamic behavior of HT-PEMEC and design control strategies. Fuzzy control strategy and neural network predictive control strategy are implemented to alleviate overshoot and suppress fluctuations so as to improve the durability of

the electrolyzer. Moreover, the neural network predictive control strategy can better suppress the overshoot and fluctuation in the dynamic process. This data-drive digital-twin model can not only guide dynamic experimental research, but also can be extended to study the dynamics of various fuel cells and electrolyzer cells.

Keywords： Proton exchange membrane electrolyzer cell; data-driven method; Numerical modelling; Dynamic research; Control strategy.

Nomenclature

Abbreviation

HT-PEMEC	High temperature proton exchange membrane electrolyzer cell
TPB	Trip phase boundary
FLC	Fuzzy logic control
MPC	Model predictive control
NNPC	Neural network predictive control
GDL	Gas diffusion layer
MSE	Mean square error

Roman

B_0	Permeability coefficient, m^2
E_{act}	Activation energy, $J \cdot mol^{-1}$
C_p	Heat capacity at constant pressure
D_i^{eff}	Effective diffusivity of species i, $m^2 \cdot s^{-1}$

D_{ik}^{eff}	Knudsen diffusion coefficient of i, $m^2 \cdot s^{-1}$
D_{im}^{eff}	Molecular diffusion coefficient of i, $m^2 \cdot s^{-1}$
i	Operating current density, $A \cdot m^{-2}$
V_{Nernst}	Equilibrium Nernst potential, V
$E_{H_2}^0$	Standard equilibrium potential for hydrogen oxidization, V
F	Faraday constant, 96485 $C \cdot mol^{-1}$
N_i	Flux of mass transport, $kg \cdot m^{-3} \cdot s^{-1}$
i_0	Exchange current density, $A \cdot m^{-2}$
n	Number of electrons transferred per electrochemical reaction
$P_{O_2}^L$	Local O_2 partial pressures, Pa
$P_{H_2}^L$	Local H_2 partial pressures, Pa
$P_{H_2O}^L$	Local H_2O partial pressures, Pa
u	Velocity field, $m^3 \cdot s^{-1}$
R	Gas constant, 8.314 $J \cdot mol^{-1} \cdot K^{-1}$
y_i	Mole fraction of component i
T	Temperature, K

1. Introduction

Sustainable energy conversion and storage technologies are eagerly needed due to the rapidly increasing energy demand and the significant ecological crisis [1-2]. Moreover, the

wide application of intermittent and fluctuating renewable energy, such as photovoltaics and wind energy, requires efficient energy storage technology for reliable power supply [3]. Hydrogen is regarded as an environmentally friendly energy carrier. It can be generated by electrolysis reaction utilising excess renewable power, and transformed back to electrical energy by a fuel cell when the electricity supply is insufficient [4-5].

Compared with alkaline water electrolyzer (AWE), proton exchange membrane electrolyzer cell (PEMEC) can generate hydrogen at a higher current density, better dynamic performance and higher hydrogen purity [6-8]. With the development in electrolyte membrane, PEMECs can be operated at a higher temperature of 120 ℃-180 ℃, enabling the use of non-noble metal catalyst [9-10]. Moreover, high temperature PEMEC (HT-PEMEC) can make good use of industrial waste heat for hydrogen production. Compared with solid oxide electrolyzer cell (SOEC) working at 700-800^{o}C, the high temperature PEMEC shows the advantage of fast start-up and better durability. Compared with room temperature PEMEC, the electrochemical performance of HT-PEMEC is enhanced due to the high temperature conditions that promote electrode kinetics [11-15]. The increased operating temperature not only reduces the need for electrical energy (reversible voltage), from 1.18 V (80 ℃) to 1.16 V (130 ℃), but also reduces the heat required for electrochemical reactions, from 284 KJ mol^{-1} (80 ℃) to 243 KJ mol^{-1} (130 ℃). Furthermore, water exists as water vapour under high temperature conditions, thus simplifying water management.

Due to its great potential for hydrogen generation, experiments and modelling were conducted to investigate the dynamic and steady-state performance of HT-PEMEC. Li et al.

[16] developed three different flow field modes (cascade, serpentine and parallel) for cathode and anode, and experimentally evaluated the influence of different flow fields on polarization loss. The cathode flow field pattern was found to only impacts the ohmic polarization of the electrode, while the anode flow field pattern significantly affected the polarization related to the catalyst layer. Wu et al. [17] experimentally evaluated the influence of operating temperature and pressure on HT-PEMEC. The current density was increased while the voltage was decreased with increasing temperature and pressure. Li et al. [18] experimentally explored the influence of operating conditions on the voltage of HT-PEMEC. It was found that increasing the temperature under the pressure of 0.1 MPa increased the concentration loss but the ohmic loss remained unchanged, and the voltage loss caused by the temperature change could be suppressed by adjusting the pressure. Natarajan et al. [19] experimentally explored the effect of different calcination temperatures on high-temperature electrolysis performance. The PEMEC calcined at 500 ℃ achieved the best performance.

Apart from experimental studies, several modeling studies were conducted on HT-PEMEC. The models for PEMEC can be classified into groups: analytical models, semi-empirical models and computational fluid dynamics (CFD) models. Among them, CFD models are widely used due to their strong interpretability and accuracy. Tijani et al. [20] built a 3D CFD model to optimize the bipolar plate of PEMEC. The optimized parallel flow field design can reduce both the pressure drop and the internal turbulence significantly. Jia et al. [21] developed a multiphysics model to study the dynamic behavior of oxygen in the electrolyzer manifold. It turns out that the pressure and gas velocity take about 2 seconds to stabilize and

the oxygen production rate and pressure drop can be adjusted by the number of channels. S.Toghyani et al. [22] proposed a finite element numerical simulation model to investigate the influence of operating conditions and structural parameters of HT-PEMEC on electrochemical performance. Bonanno et al. [23] evaluated the energy efficiency and exergy efficiency of PEMEC from a system perspective. The high system efficiency was due to the high heat utilization rate under thermally neutral conditions. Ruiz et al. [24] built a CFD model to investigate the effects of three different flow channel configurations (serpentine, multiple serpentine and parallel) on the performance of the electrolytic cell. The results show that the multiple-serpentine flow channel has better performance in terms of temperature uniformity and hydrogen generation. Toghyani et al. [25] proposed a non-isothermal model based on the finite volume method for efficiency and exergoeconomic analysis. The higher temperature was found to reduce the cost of the HT-PEMEC and increase the exergy efficiency, and the high-pressure operating condition also promote cost reduction.

Based on the above literature survey, it is clear that the current research focuses on the influence of operating conditions and structural parameters on the performance of HT-PEMEC, while the dynamic behaviour is rarely studied. The rapid electrochemical reaction easily causes overshoot and fluctuations in the dynamic behavior, which leads to a decrease in system durability. Therefore, the research of dynamic processes is necessary. As shown in Fig. 1a, experimental testing is very time consuming, expensive, and cannot provide detailed information in the electrolyzer cell. Multiphysics modeling can provide detailed information but it is computationally demanding. The method of combining the multiphysics model with

system identification is thus proposed to study the dynamic process of the nonlinear dynamic system to achieve both high accuracy and low computational cost. The dynamic research framework is presented in Fig. 1b. The multiphysics model was developed and validated to investigate the performance of HT-PEMEC. Datasets of dynamic behaviour are generated by adjusting the input of the multiphysics model. Then the datasets are used for system identification. The identification model is verified by comparison with the multiphysics model. Subsequently, the identification model is used to design control strategies. This method can also be extended to other dynamic studies of fuel cells and electrolyzer cells.

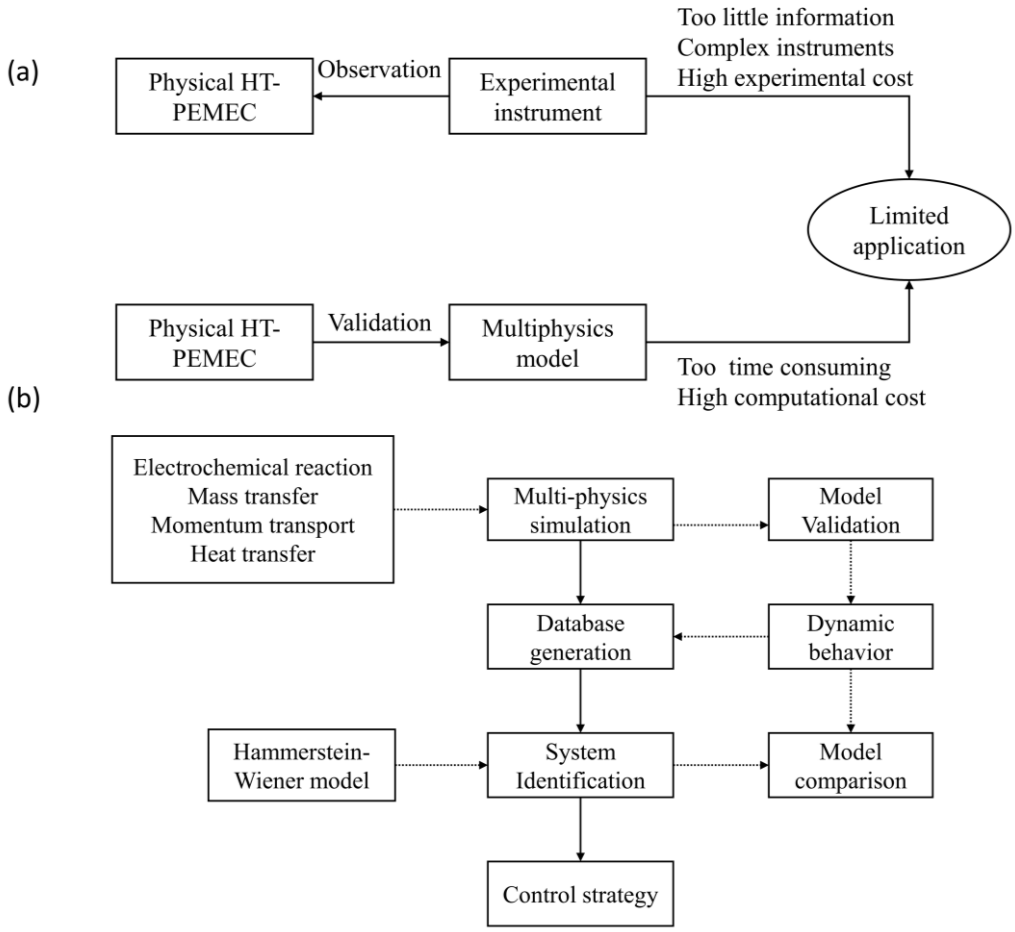

Fig. 1. (a) The application limitations of experimental observation and multiphysics model; (b) Data-driven dynamic research framework.

2. Multi-physics model description

The two-dimensional multiphysics model has been developed to explore the dynamic processes, including electrochemical reaction, temperature distribution, mass/momentum transportation and electron/ion conduction [30]. The schematic diagram of HT-PEMEC is shown in Fig. 2. In operation, water steam is introduced into the cathode and anode. The steam at the cathode side serves as a carrier gas. Gaseous H_2O molecules transport through the porous anode to TPB, generating oxygen, hydrogen protons and electrons. Hydrogen protons diffuse through the membrane to the catalytic layer of the cathode, and combine with electrons to produce hydrogen molecules. The detailed model parameters are listed in Table 1.

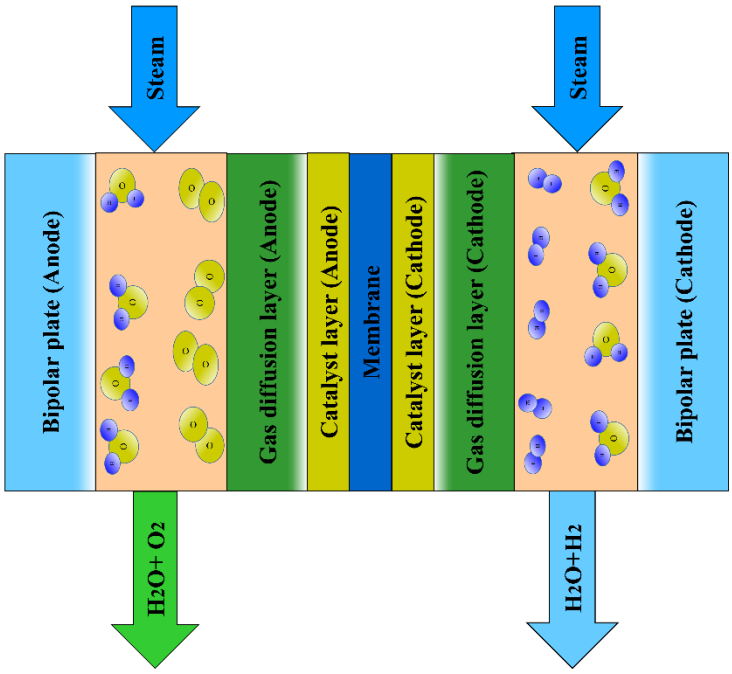

Fig.2. Schematic figure of the HT-PEMEC.

Table 1. Physical and geometric parameters of the model.

Parameter	value	unit
Channel height	1	mm
Channel length	50	mm

Membrane thickness	0.1	mm
Catalyst layer thickness	0.05	mm
Gas diffusion layer thickness	0.38	mm
Operating temperature	403.15	K
Operating pressure	1	bar
Porosity of catalyst layer	0.3	
GDL porosity	0.4	
Catalyst layer permeability	2.36×10^{-12}	m^2
GDL permeability	1.18×10^{-11}	m^2
Anode exchange current density	10^{-4}	A cm^{-2}
Cathode exchange current density	0.1	A cm^{-2}
Anode gas flow rate	0.2	m s^{-1}
Cathode gas flow rate	0.2	m s^{-1}
Proton conductivity of electrolyte	20	S m^{-1}

2.1 Model assumption

The following assumptions are utilized in the finite element method.

(1) All porous materials are isotropic and homogeneous;

(2) All gases (H_2O, H_2, O_2) in the multi-physics model are regarded as ideal gases;

(3) TPB is evenly distributed in the porous catalyst layer.

2.2 Electrochemical reaction

In this model, the electrolysis reaction of the anode and cathode is written as Eq. (1) and (2).

$$\text{Anode: } 2H_2O \rightarrow O_2 + 4H^+ + 4e^- \quad (1)$$

$$\text{Cathode: } 2H^+ + 2e^- \rightarrow H_2 \quad (2)$$

Equilibrium potential of the electrochemical reaction can be calculated as follows.

$$V_{Nernst} = E^0_{H_2} + \frac{RT}{2F} ln \left[\frac{P^L_{H_2} \left(P^L_{O_2}\right)^{1/2}}{P^L_{H_2O}} \right] \quad (3)$$

Here $E^0_{H_2}$ represents the standard potential of the electrochemical reaction. $P^L_{H_2}$, $P^L_{H_2O}$ and $P^L_{O_2}$ represent the local pressure of various gases. Moreover, the local gas partial pressure at TPB is used, thereby the concentration loss is incorporated in the equilibrium potential Eq. (3).

The operating voltage applied to the electrodes of the electrolyzer is expressed as Eq. (4).

$$V_{cell} = V_{Nernst} + \eta_{act} + \eta_{ohm} \quad (4)$$

The activation overpotential (η_{act}) represents the energy barrier of the electrolysis reaction on the porous electrode, which is mainly related to the electrode material and microstructure. The activation overpotential can be expressed by the Buttler-Volmer equation.

$$i = i_0 \left\{ exp\left(\frac{\alpha n F \eta_{act}}{RT}\right) - exp\left(\frac{(1-\alpha) n F \eta_{act}}{RT}\right) \right\} \quad (3)$$

$$i_0 = \gamma \exp(-\frac{E_{act}}{RT}) \quad (4)$$

Here α represents the transfer coefficient, n represents the number of transferred electrons, E_{act} denotes the activation energy of the electrochemical reaction, γ denotes the pre-exponential factor of Eq. (4).

The ohmic overpotential (η_{ohm}) is caused by the resistance of proton and electron transport in the electrolyzer, which usually is expressed by the Ohm law.

2.3 Fluid flow and mass transport

The mass transport of various gases in porous media and channels is described by Eq. (5) and Eq. (6) [26].

$$N_i = -\frac{1}{RT}\left(\frac{B_0 y_i P}{\mu}\nabla P - D_i^{eff}\nabla(y_i P)\right) \text{ (i=1,2,…..n)} \quad (5)$$

$$D_i^{eff} = \frac{\varepsilon}{\tau}\left(\frac{1}{D_{im}^{eff}} + \frac{1}{D_{ik}^{eff}}\right) \quad (6)$$

Here N_i represents the mass transfer flux of component i, y_i represents the molar fraction of i, B_0 represents permeability coefficient, μ is gas viscosity, τ is tortuosity, ε is porosity. Furthermore, the mass conservation is expressed as Eq. (7).

$$\nabla\left(-D_i^{eff}\nabla C_i\right) = R_i \quad (7)$$

Here C_i and R_i are the mole concentration and the mass source term of component i, respectively.

Navier-Stokes equation is utilised to calculate the momentum transfer in porous media and channels [27].

$$\rho\frac{\partial \mathrm{u}}{\partial \mathrm{t}} + \rho \mathrm{u}\nabla \mathrm{u} = -\nabla \mathrm{p} + \nabla\left[\mu(\nabla \mathrm{u} + (\nabla \mathrm{u})^T) - \frac{2}{3}\mu\nabla \mathrm{u}\right] - \frac{\varepsilon\mu \mathrm{u}}{B_0} \quad (8)$$

Here u and ρ is the velocity vector and gas density. Table 2 lists the physical parameters of various gases.

Table 2. Physical properties of gaseous components [28].

Parameter	Value
Viscosity of H_2O	(-36.826+4.29e^{-1}•T-1.62 e^{-5}•T^2)•1e^{-7} [Pa•s]
Viscosity of H_2	(27.758+2.12e^{-1}•T-3.28e^{-5}•T^2)•1e^{-7} [Pa•s]
Viscosity of O_2	(44.224+5.62e^{-1}•T-1.13e^{-5}*T^2)•1e^{-7} [Pa•s]
Heat capacities of H_2O	33.93-8.42e^{-2}•T+2.99e^{-5}•T^2-1.78e^{-8}•T^3+ 3.69e^{-12}•T^4 [J/mol•K]

Heat capacities of H_2	$25.4+2.02e^{-2} \cdot T-3.85e^{-5} \cdot T^2+3.19e^{-8} \cdot T^3-8.76e^{-12} \cdot T^4$ [J/mol•K]
Heat capacities of O_2	$29.53-8.90e^{-2} \cdot T+3.81e^{-5} \cdot T^2-3.26e^{-8} \cdot T^3+ 8.86 \cdot e^{-12} * T^4$ [J/mol•K]
Thermal conductivities of H_2O	$0.53e^{-3}+4.71e^{-4} \cdot T+4.96e^{-8} \cdot T^2$ [W/m/K]
Thermal conductivities of H_2	$0.36e^{-1}+4.59e-^{4} \cdot T-6.49e^{-8} \cdot T^2$ [W/m/K]
Thermal conductivities of O_2	$0.12e^{-2}+8.62e^{-4} \cdot T-1.33e^{-8} \cdot T^2$ [W/m/K]

2.4 Temperature field model

The electrochemical reaction is endothermic but the overpotential loss is exothermic, and the temperature distribution can be calculated by the heat balance equation as Eq. (8) and Eq. (9) [29].

$$\rho C_p u \bullet \nabla T + \nabla\left(-\lambda_{eff} \nabla T\right) = Q \tag{8}$$

$$\lambda_{eff} = (1-\varepsilon)\lambda_s + \varepsilon\lambda_g \tag{9}$$

Here C_p is the fluid heat capacity, u is the flow rate, λ_{eff} is the effective thermal conductivity, λ_s represents the solid thermal conductivity, λ_g represents gaseous thermal conductivity. Q represents heat source, including heat generation (Q_{Gen}) due to overpotential loss and heat consumption (Q_{Con}) due to electrolysis reaction.

$$\begin{cases} Q_{Gen} = E_{Irr} \times \mathrm{i} \\ Q_{Con} = T\Delta S = \Delta H - \Delta G \end{cases} \tag{10}$$

Here E_{Irr} is overpotential, ΔS and ΔH are the entropy change and reaction enthalpy,

ΔG represents the Gibbs free energy.

2.5 Boundary conditions and validation

Both the cathode and anode of HT-PEMEC are open-end. The operating voltage is applied to the outer surfaces of the anode and cathode. Back gas pressure is specified as 1 atm. The operating temperature and flow rate of the anode and cathode inlets are specified. The walls are adiabatic. The time step of the dynamic solver is set to 0.01s. The multiphysics model was solved utilising the finite element method. More details about the model and the model validation can be found in ref. [30, 35].

3. Dynamic system identification

Multiphysics model can provide more accurate results than analytical models and semi-experimental models, thus it is widely used to analyze the dynamic and static behaviour of electrolyzer cells and fuel cells. However, the calculation process of the multiphysics model is time-consuming, thereby it is not suitable for real-time control purpose. Transfer functions or state equations are obtained which are necessary for complex control strategies, such as robust control and predictive control. The transfer functions identified from the multiphysics model is a very efficient method. It not only ensures the accuracy of the model but also improves computational efficiency.

The measured data is required to adequately reflect the dynamic behaviour of the system to identify an accurate model. Therefore, the dynamic behaviour between random non-periodic steady-state operating points is measured, and the time interval of the step response allows the

dynamic process to reach a steady-state to obtain a time constant. Fig. 3 shows the identification and validation data obtained from the multiphysics model. Identification data and validation data are collected by adjusting the operating voltage, and the anode flow rate was sufficiently large to suppress reactant starvation during the dynamic process. The data is acquired with a sampling interval of 0.01 s and a duration of 1200 s. Furthermore, two sets of dynamic data are obtained from the multiphysics model, one set of data is used to identify the transfer functions model and the other set of data is used for validation.

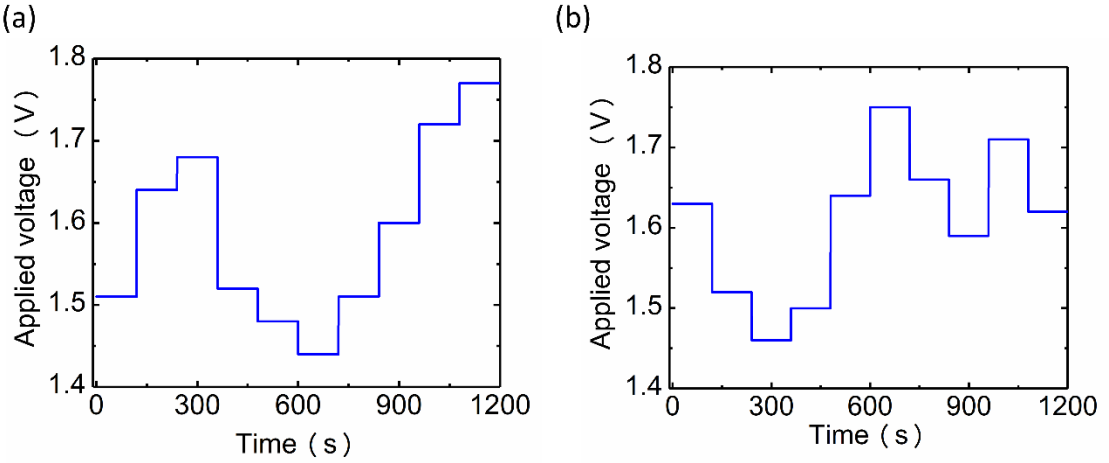

Fig. 3. (a) The voltage adjustment in identification data; (b) The voltage regulation in validation data.

The transfer function model was identified from the identification data using System Identification Toolbox™ of Matlab. The research focuses on identifying the dynamic behaviour of the electrolytic cell without considering a specific mathematical structure, hence the black-box identification technique is chosen. However, black-box modelling is generally an error-and-trial process, thus the structure and parameters of the model are estimated and compared to determine model accuracy. System identification usually starts with a linear structural model

and attempts to use higher order models or non-linear structures when the fit is poor. The method of system identification is regarded as a single-input single-output (SISO) model to reduce the coupling between different sub-models to improve identification accuracy. The power consumption sub-model, the hydrogen generation sub-model and the temperature sub-model were developed to study the control strategy in the dynamic process and calculate the electrolysis efficiency.

The efficiency of an HT-PEMEC can be determined as a ratio of input energy to output energy. The input energy includes the input electrical energy and the input thermal energy for heating gas, and the output energy is the chemical energy produced [31].

$$\eta = \frac{(\dot{m}_{o,H_2} - \dot{m}_{i,H_2}) LHV_{H_2}}{V \int_0^{L_{RU}} i dz + \dot{m}_{i,ca} \int_{T_0}^{T_{i,ca}} C_{p,g,ca} dT + \dot{m}_{i,an} \int_{T_0}^{T_{i,an}} C_{p,g,an} dT} \tag{11}$$

Where $\dot{m}_{i,H_2}$ and $\dot{m}_{o,H_2}$ are hydrogen mass flow rate at inlet and outlet. $\dot{m}_{i,ca}$ and $\dot{m}_{i,an}$ denote the cathode and anode gas mass flow rates, respectively. $C_{p,g,ca}$ and $C_{p,g,an}$ represent the cathode and anode gas heat capacities.

3.1 Identification results

The structure and order of the linear model are obtained by trial and error, and the general output-error (OE) model is represented as Eq. (12) [32].

$$\mathrm{y(t)} = \frac{B(z)}{F(z)} u(t-n) + e(t) \tag{12}$$

Here u(t) denotes system input, y(t) denotes the system output, e(t) denotes system disturbance, n indicates system delay. $\mathrm{F(z)}$ and $\mathrm{B(z)}$ are polynomials with regard to the z^{-1} operator, respectively.

$$\begin{cases} B(z) = b_0 + b_1 z^{-1} + b_2 z^{-2} + \cdots + b_{kb-1} z^{-(kb-1)} \\ F(z) = 1 + f_1 z^{-1} + f_2 z^{-2} + \cdots + f_{kf} z^{-kf} \end{cases} \quad (13)$$

HT-PEMEC is a non-linear system and therefore non-linear factors need to be added to the linear model. Hammerstein-Wiener models are generally used to describe the dynamic behaviour of non-linear systems. As shown in Fig. 4, the Hammerstein-Wiener model consists of a linear block, an input nonlinearity and an output nonlinearity. The linear block is used to describe the dynamics of the modeled system, while the input nonlinearity and output nonlinearity are used to reflect the nonlinear characteristics of the system.

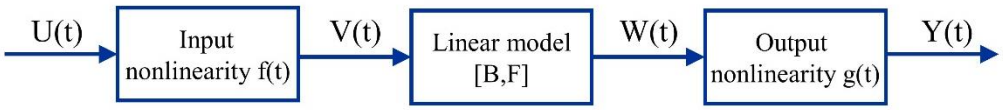

Fig. 4. Hammerstein-Wiener model framework

The accuracy of the fit can be described as Eq. (14).

$$\text{Fit} = \left(1 - \frac{\|y - \hat{y}\|}{\|y - \hat{y}\|}\right) \times 100\% \quad (14)$$

Here y represents the output of multiphysics data, $\hat{y}$ denotes the output of the identification model. $\bar{y}$ denotes the average of y.

The mean squared error (MSE) is also used to validate the model and is expressed as Eq. (15).

$$\text{MSE} = \frac{1}{N}\sum_{j=1}^{N}(y - \hat{y})^2 \quad (15)$$

Here N denotes the total number of data, and j represents the jth output result.

3.1.1 Applied voltage versus power consumption sub-model

System dynamics are first obtained by identifying linear systems to determine the coefficients of B and F. Subsequently, the best performance was observed by describing the input nonlinearity and the output nonlinearity using segmented functions and one-dimensional polynomials respectively. The voltage versus power consumption sub-model can be expressed as Eq. (16).

$$\begin{cases} f(t) = \begin{cases} 2.54u(t) - 3.849 & 0 \ll u(t) < 1.65 \\ 4.065u(t) - 6.367 & u(t) \geq 1.65 \end{cases} \\ \begin{cases} w(t) = \left[\frac{\mathrm{B(z)}}{\mathrm{F(z)}}\right] v(t) + e(t) \\ \mathrm{B(z)} = z^{-1} - 0.9918z^{-2} \\ \mathrm{F(z)} = 1 - 0.9372z^{-1} - 0.0077z^{-2} - 0.0452z^{-3} \end{cases} \\ g(t) = 5.1478E^3 w(t)^2 + 2.2109E^3 w(t) + 315.6857 \end{cases} \tag{16}$$

Here u(t) is applied voltage, y(t) is power density (W m^{-2}). Fig. 5 shows the results of the identification and validation data compared to the output of the identification model. The power consumption sub-model is able to describe the system dynamics and the corresponding evaluation indicators are listed in Table 3.

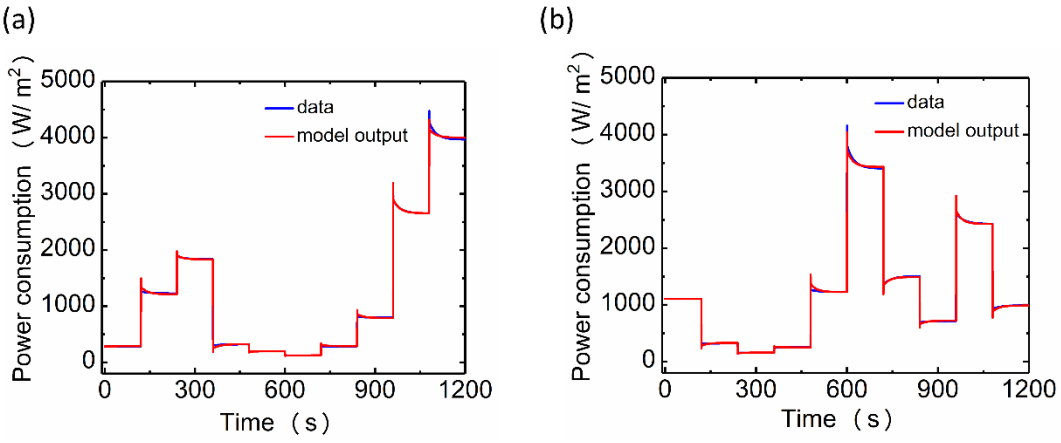

Fig. 5. (a) Comparison of identification model output and identification data; (b)

Comparison of identification model output and validation data

3.1.2 Applied voltage versus hydrogen generation sub-model

The hydrogen generation sub-model has a similar structure to the power consumption sub-model because the hydrogen generated is proportional to the current density. Therefore, the best performance is obtained by selecting the piecewise function to describe the input nonlinearity and the one-dimensional polynomial to describe the output nonlinearity, respectively. The voltage versus hydrogen generation sub-model can be expressed as Eq. (17).

$$\begin{cases} f(t) = \begin{cases} 1.448u(t) - 2.197\ 0 \ll u(t) < 1.62 \\ 1.966u(t) - 3.035\ u(t) \geq 1.62 \end{cases} \\ \begin{cases} w(t) = \left[\frac{\mathrm{B(z)}}{\mathrm{F(z)}}\right] v(t) + e(t) \\ \mathrm{B(z)} = z^{-1} - 0.9926z^{-2} \\ \mathrm{F(z)} = 1 - 1.17183z^{-1} + 0.8562z^{-2} - 0.1345z^{-3} \end{cases} \\ g(t) = 1.7556E^{-4}w(t)^2 + 1.1739E^{-4}w(t) + 3.1594E^{-5} \end{cases} \tag{17}$$

Here u(t) is applied voltage, y(t) is hydrogen generated (kg m^{-2} s^{-1}). As shown in Fig. 6, the identification model output is compared with the identification and validation data to verify the hydrogen generation sub-model. Furthermore, the performance indicators are summarized in Table 3.

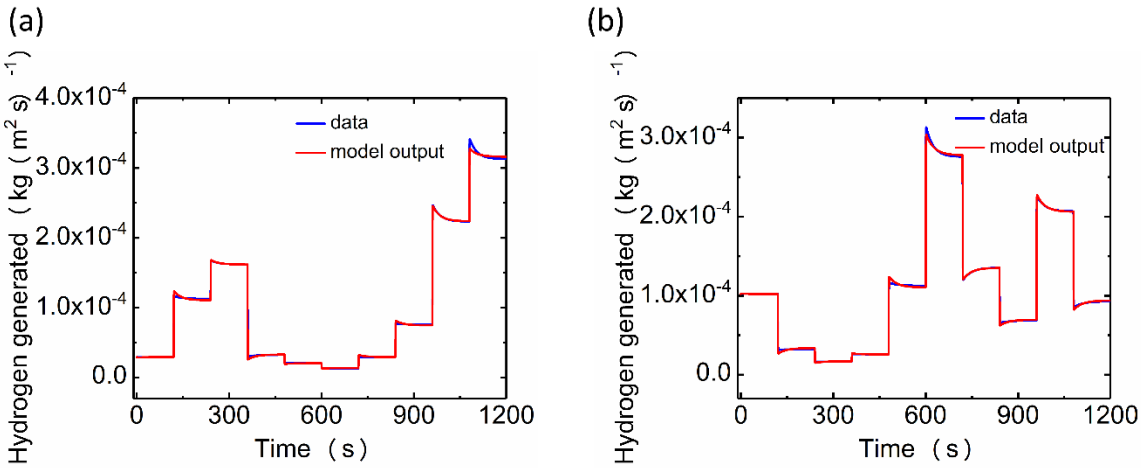

Fig. 6. (a) Comparison of identification model output and identification data; (b) Comparison of identification model output and validation data

3.1.3 Applied voltage versus temperature sub-model

Heat transfer is slow compared to the dynamics of other physical parameters and the model has high delays and strong non-linearity. The best performance of the identification model was observed through the use of segmentation functions and one-dimensional polynomials to describe input nonlinearity and output nonlinearity. The voltage versus temperature sub-model can be expressed as Eq. (18).

$$\begin{cases} f(t) = \begin{cases} 0.1296u(t) - 0.2225 \; 0 \ll u(t) < 1.61 \\ 0.5676u(t) - 0.9277 \; u(t) \geq 1.61 \end{cases} \\ \begin{cases} w(t) = \left[\frac{\mathrm{B(z)}}{\mathrm{F(z)}}\right] v(t) + e(t) \\ \mathrm{B(z)} = -0.422z^{-1} + z^{-2} - 0.4538z^{-3} - 0.7063z^{-4} + 0.8802z^{-5} - 0.2982z^{-6} \\ \mathrm{F(z)} = 1 - 3.1524z^{-1} + 3.0392z^{-2} + 0.6171z^{-3} - 3.3842z^{-4} + 2.5233z^{-5} - 0.643z^{-6} \end{cases} \\ g(t) = 29.7651w(t)^2 - 17.5995w(t) + 414.9453 \end{cases} \tag{18}$$

Here u(t) is applied voltage, y(t) denotes operating temperature (K). Fig. 7 shows the comparison of the identification and validation data with the model output. The temperature identification model has a lower fit compared to the power consumption sub-model and the hydrogen generated sub-model, due to the high latency and strong non-linearity of the temperature model. However, the errors are acceptable and the corresponding evaluation indicators are listed in Table 3.

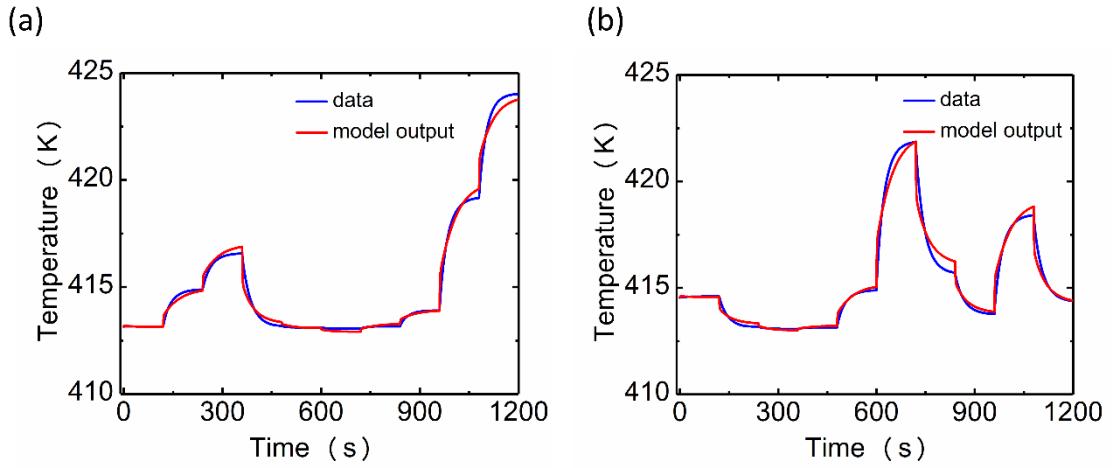

Fig. 7. (a) Comparison of identification model output and identification data; (b) Comparison of identification model output and validation data

Table 3. Identification model evaluation index.

Indicator	Power consumption sub-model		Hydrogen generated sub-model		Temperature sub-model	
	Identification data	Validation data	Identification data	Validation data	Identification data	Validation data
Fit (%)	97.57	96.31	98.1	97.87	92.66	87.73
MSE	0.913	1.352	$6.253E^{-12}$	$9.918\ E^{-12}$	0.1011	0.2295

4. Dynamic control strategy

The utilization of excess renewable energy to produce hydrogen for subsequent fuel cells and industrial applications is the most promising pathway for HT-PEMEC. However, the fast

electrochemical response easily triggers excessive overshoot and fluctuation, resulting in poor durability and dynamic performance. Therefore, dynamic research is necessary for long-term stable operation. Dynamic multi-physics models can be used to analyze the dynamic behaviour of electrolyzer cells to develop control strategies. Subsequently, the performance of the control strategy can be verified in the identified dynamic system to provide a reference for the experiment.

4.1 Dynamic behaviour

The dynamic process of HT-PEMEC can be divided into two stages, namely, rapid electrochemical response and relatively slow mass transfer process. As shown in Fig. 8, the transient process of the operating voltage from 1.6 V to 1.7 V.

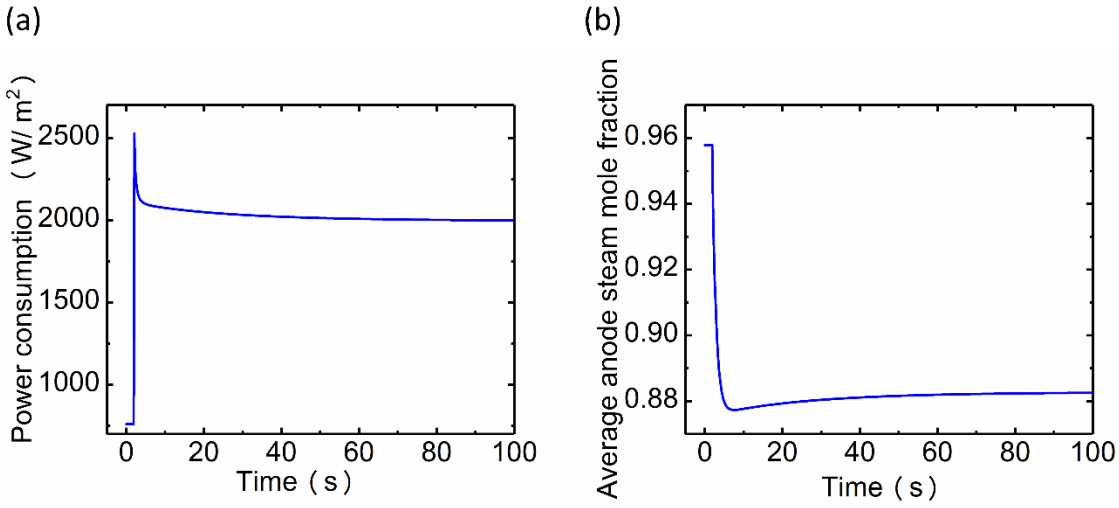

Fig. 8. (a) Dynamic response of power consumption; (b) Dynamic response of steam mole fraction in the catalytic layer.

An obvious overshoot exists in the dynamic process of power response. The power consumption rises rapidly due to the fast electrochemical response, however, the relatively slow

mass transfer process leads to a rapid decrease in the reactant concentration, which eventually causes the power consumption to drop to a steady state. To alleviate overshoot and fluctuation, it is essential that the electrochemical response be adjusted during the dynamic process.

4.2 Fuzzy logic control strategy

Fuzzy logic control (FLC) strategy is a rule-based nonlinear control method. Moreover, the main advantage of the method can be applied to dynamic systems where models are difficult to obtain, and inference rules can be designed based on the experience of human experts [33]. The 2D FLC can adjust the control strategy according to the error and the change of the error in real time, and its work flow is shown in Fig. 9. The fuzzification process uses membership functions to convert precise input into fuzzy language, and then calculates the output through pre-set inference rules, lastly, the output is converted into precise control parameters by defuzzification.

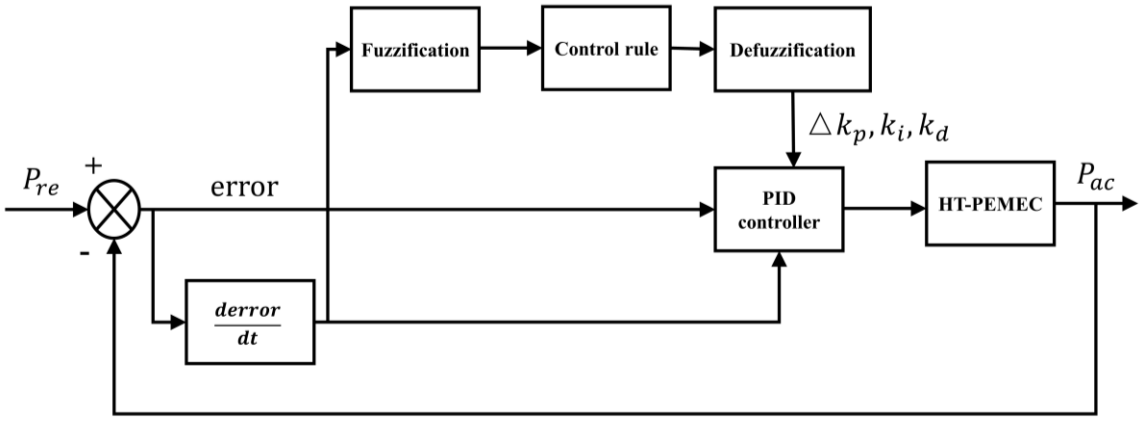

Fig. 9. The 2D fuzzy logic controller framework

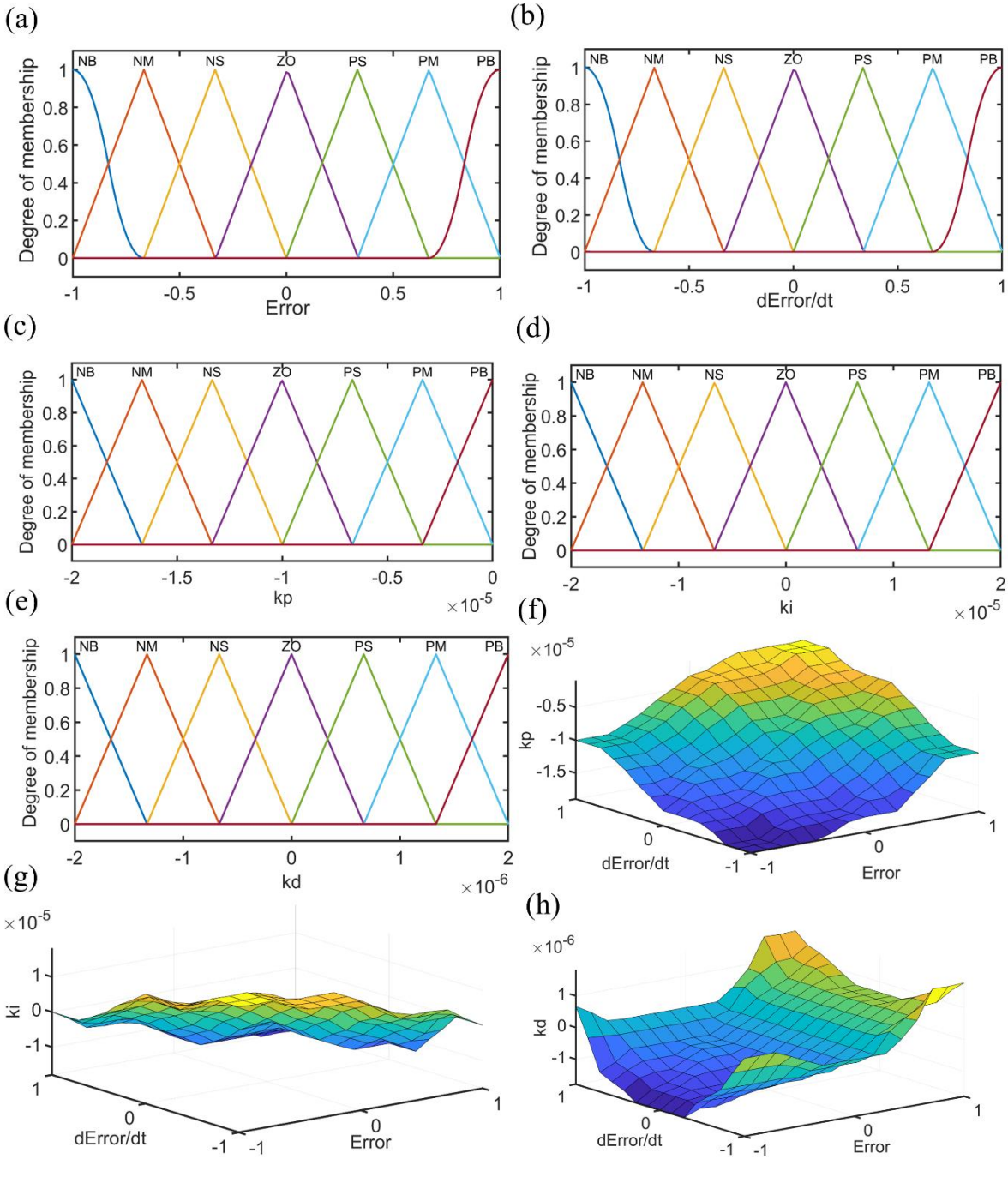

Fig. 10. (a) Membership function of the error; (b) Membership function of the change of error; (c) Membership function of the change of k_p; (d) Membership function of the change of k_i; (e) Membership function of the change of k_d; (f) Output characteristic of the change of k_p; (g) Output characteristic of the change of k_i; (h) Output characteristic of the change of k_d;

Here P_{re} is the reference power, P_{ac} is the actual power density. Δk_p, Δk_d and Δk_i are the changes in the control coefficients respectively. This fuzzy logic block has three outputs and two inputs; the inputs represent the error and the change of error, and the outputs are the changes in k_p, k_d and k_i respectively. The fuzzy subsets of output and input are divided into {NB, NM, NS, ZO, PS, PM, PB}. Moreover, the output characteristics and membership function are shown in Fig. 10. The fuzzy logic control strategy is applied as the control signal is initially enhanced to accelerate the dynamic response and subsequently reduced to suppress overshoot.

4.3 Neural Network Predictive Control Strategy

Model predictive control is a nonlinear control strategy based on model prediction and online optimization. Moreover, model predictive control has a wider control horizon due to the ability to predict dynamic behavior compared to other control strategies [34]. The neural network predictive control (NNPC) strategy uses a non-linear neural network to predict the dynamic behavior of the HT-PEMEC, thereby optimizing the dynamic behavior to reduce overshoot. The detailed workflow of NNPC is shown in Fig. 11 and specific implementation steps can refer to the Deep Learning Toolbox of Matlab.

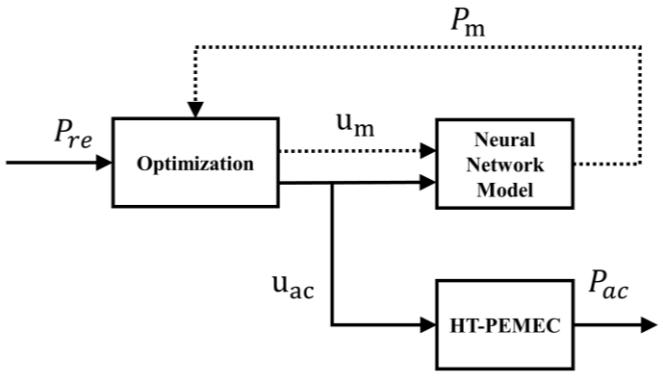

Fig. 11. The Neural network predictive control framework

Here $\mathrm{P_m}$ is the predictive model output, $\mathrm{u_m}$ is the predictive model input and $\mathrm{u_{ac}}$ is the actual electrolyzer input. The optimization is implemented through the calculation of Eq. 20, and then the optimized input voltage $\mathrm{u_{ac}}$ is supplied to the electrolyzer to optimize the dynamic process.

$$\mathrm{J} = \sum_{j=1}^{N_p}[P_{re}(k+j) - P_m(k+j)]^2 + \rho\sum_{j=1}^{N_c}[u_m(k+j-1) - u_m(k+j-2)]^2 \qquad (20)$$

Here N_c represents the control time domain length, N_p represents the predicted time domain length and ρ is the weighting factor. Optimization is performed by calculating the minimum value of J. NNPC adjusts the operating voltage by predicting the dynamic behavior of HT-PEMEC to alleviate overshoot and fluctuation.

4.4 Results and analysis

Fuzzy logic control strategy and neural network predictive control strategy are applied in the dynamic process of HT-PEMEC to suppress overshoot and fluctuation. The random variation of power consumption is used to represent renewable energy, with an interval of 30 seconds and a sampling interval of 0.01s. Furthermore, the dynamic response and control

strategy of the electrolyzer were compared, as shown in Fig. 12.

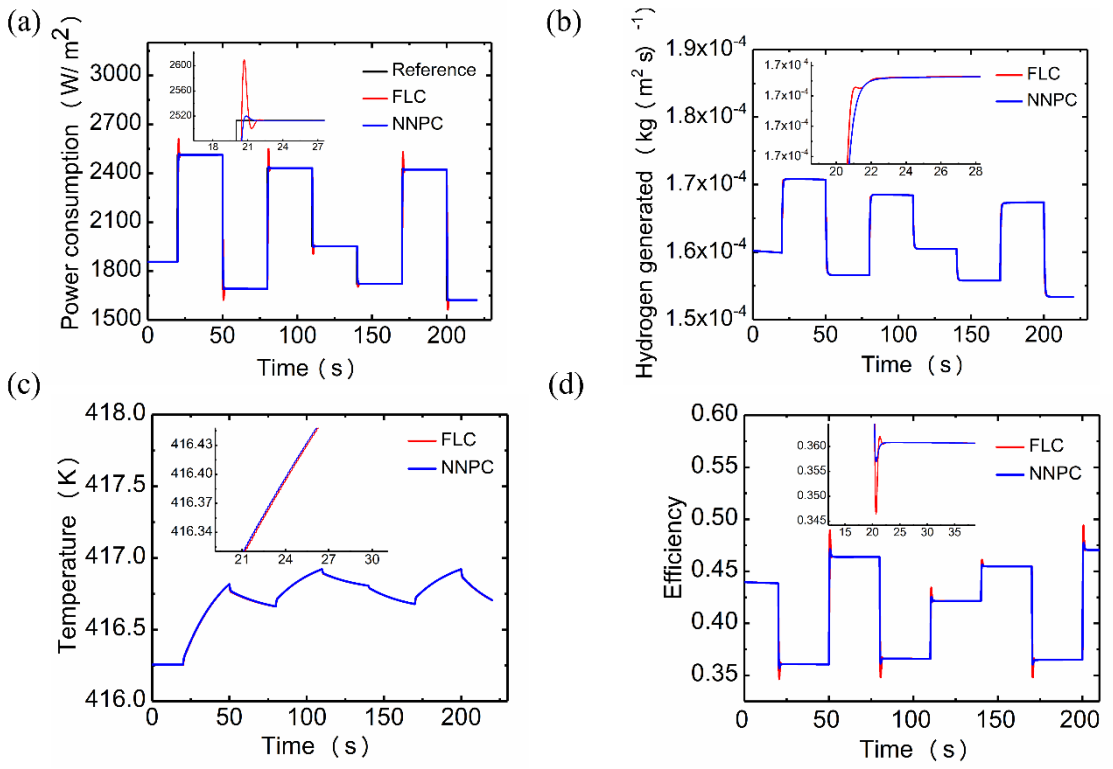

Fig.12. (a) Dynamic response of power consumption; (b) Dynamic response of hydrogen generated; (c) Dynamic response of temperature; (d) Efficiency changes in dynamic processes.

The dynamic behavior of energy consumption is shown in Fig. 12a. Neural network predictive control strategy shows better dynamic performance and smaller overshoot compared to the fuzzy control strategy. Neural network predictive control can predict the dynamic behaviour of HT-PEMEC for online optimization, compared with the fuzzy logic control strategy optimized based on real-time error and error change rate, it has a wider control horizon. The fuzzy logic control strategy calculates the controller output according to the pre-made fuzzy inference rules, which requires fewer calculation resources than online calculation. The hydrogen generation rate in the dynamic process is shown in Fig. 12b. The hydrogen

production rate in the fuzzy control strategy is greater than the neural network predictive control strategy due to the dramatic power consumption increase and excessive overshoot in the initial phase of the dynamic process, the subsequent two control strategies maintain the same hydrogen production rate. The temperature response of neural network predictive control is similar to the fuzzy logic control strategy, and the results are shown in Fig. 12c. The dynamic efficiency calculation can be divided into the input electric energy, the heating gas energy, and the chemical energy produced. As shown in Fig. 12b and Fig. 12c, There is little difference between the energy of heating gas and the chemical energy produced in the dynamic process, thus the fluctuation of efficiency is mainly affected by the input electric energy. It can be observed from Fig. 12d that the fluctuation of the efficiency during the dynamic process corresponds to the overshoot of the power consumption. Overall, neural network predictive control strategies can provide better dynamic performance.

Conclusions

Traditional experimental observations require complex instruments and high experimental costs to study the dynamic process of HT-PEMEC. Moreover, the widely used multiphysics model is time-consuming and requires a lot of computing resources. The data-driven dynamic research method is proposed by combining multiphysics models and system identification methods. A 2D multiphysics simulation model was established to study the electrolyzer cell, in which electrochemistry, mass transfer, momentum transfer and heat transfer were considered.

Subsequently, the dynamic data generated by the multiphysics model is used for system identification. Furthermore, The identification model is verified by comparison with the multiphysics model.

To predict the dynamic behaviour of HT-PEMEC and calculate the efficiency in the dynamic process, the power consumption sub-model, the hydrogen generation sub-model and the operating temperature sub-model are identified. Fuzzy logic control strategy and neural network predictive control strategy are designed to control power consumption to improve dynamic behavior. Neural network predictive control shows better dynamic performance and smaller overshoot compared to fuzzy logic control strategies, but it requires more computing resources.

This data-driven approach provides a promising solution by combining multiphysics models and system identification, which can quickly and accurately analyze the performance of nonlinear dynamic systems. Currently, this method is only used in the single-input single-output system, and then can be applied to a multiple-input multiple-output system and consider the coordinated control of multiple physical parameters.

Acknowledgments

M. NI thanks the grants (Project Number: PolyU 152064/18E and N_PolyU552/20) from Research Grant Council, University Grants Committee, Hong Kong SAR.

References

[1] Luo X, Wang J, Dooner M, et al. Overview of current development in electrical energy storage technologies and the application potential in power system operation[J]. Applied energy, 2015, 137: 511-536.

[2] Su Y W. Residential electricity demand in Taiwan: Consumption behavior and rebound effect[J]. Energy Policy, 2019, 124: 36-45.

[3] Dincer I. Renewable energy and sustainable development: a crucial review[J]. Renewable and sustainable energy reviews, 2000, 4(2): 157-175.

[4] Tarhan C, Çil M A. A study on hydrogen, the clean energy of the future: Hydrogen storage methods[J]. Journal of Energy Storage, 2021, 40: 102676.

[5] Dafedar A A, Verma S S, Yadav A. Hydrogen Storage Techniques for Stationary and Mobile Applications: A Review[J]. Recent Advances in Sustainable Technologies, 2021: 29-40.

[6] Schmidt O, Gambhir A, Staffell I, et al. Future cost and performance of water electrolysis: An expert elicitation study[J]. International Journal of Hydrogen Energy, 2017, 42(52): 30470-30492.

[7] Rahim A H A, Tijani A S, Kamarudin S K, et al. An overview of polymer electrolyte membrane electrolyzer for hydrogen production: Modeling and mass transport[J]. Journal of Power Sources, 2016, 309: 56-65.

[8] Ni M, Leung M K H, Leung D Y C. Energy and exergy analysis of hydrogen production by a proton exchange membrane (PEM) electrolyzer plant[J]. Energy conversion and management, 2008, 49(10): 2748-2756.

[9] Bose S, Kuila T, Nguyen T X H, et al. Polymer membranes for high temperature proton exchange membrane fuel cell: recent advances and challenges[J]. Progress in Polymer Science, 2011, 36(6): 813-843.

[10] Shao Y, Yin G, Wang Z, et al. Proton exchange membrane fuel cell from low temperature to high temperature: material challenges[J]. Journal of Power Sources, 2007, 167(2): 235-242.

[11] Nikiforov AV, Garcı´a ALT, Petrushina IM, et al. Preparation and study of IrO2/SiC-Si supported anode catalyst for high temperature PEM steam electrolysers[J]. International Journal of Hydrogen Energy, 2011,36(10):5797-805

[12] Nikiforov A V, Petrushina I M, Christensen E, et al. WC as a non-platinum hydrogen evolution electrocatalyst for high temperature PEM water electrolysers[J]. International journal of hydrogen energy, 2012, 37(24): 18591-18597.

[13] Nikiforov A, Christensen E, Petrushina I, et al. Advanced construction materials for high temperature steam PEM electrolysers[J]. Electrolysis; Linkov, V., Kleperis, J., Eds.; IntechOpen: London, UK, 2012: 61-86.

[14] Hansen MK, Bjerrum N, Christensen E, Jensen JO. PEM water electrolysis at elevated temperatures. Ph.D. thesis. Technical University of Denmark, Department of Chemistry Institut;2012.

[15] Aili D, Hansen M K, Pan C, et al. Phosphoric acid doped membranes based on Nafion®, PBI and their blends–Membrane preparation, characterization and steam electrolysis testing[J]. international journal of hydrogen energy, 2011, 36(12): 6985-6993.

[16] Li H, Nakajima H, Inada A, et al. Effect of flow-field pattern and flow configuration on the performance of a polymer-electrolyte-membrane water electrolyzer at high temperature[J]. International Journal of Hydrogen Energy, 2018, 43(18): 8600-8610.

[17] Xu W, Scott K, Basu S. Performance of a high temperature polymer electrolyte membrane water electrolyser[J]. Journal of Power Sources, 2011, 196(21): 8918-8924.

[18] Li H, Inada A, Fujigaya T, et al. Effects of operating conditions on performance of high-temperature polymer electrolyte water electrolyzer[J]. Journal of Power Sources, 2016, 318: 192-199.

[19] Natarajan V, Basu S, Scott K. Effect of treatment temperature on the performance of RuO2 anode electrocatalyst for high temperature proton exchange membrane water electrolysers[J]. International journal of hydrogen energy, 2013, 38(36): 16623-16630.

[20] Tijani A S, Barr D, Rahim A H A. Computational modelling of the flow field of an electrolyzer system using CFD[J]. Energy Procedia, 2015, 79: 195-203.

[21] Jia Y, Zeng M, Barnoon P, et al. CFD simulation of time-dependent oxygen production in a manifold electrolyzer using a two-phase model[J]. International Communications in Heat and Mass Transfer, 2021, 126: 105446.

[22] Toghyani S, Afshari E, Baniasadi E, et al. Thermal and electrochemical performance assessment of a high temperature PEM electrolyzer[J]. Energy, 2018, 152: 237-246.

[23] Bonanno M, Mueller K, Bensmann B, et al. Evaluation of the Efficiency of an Elevated Temperature Proton Exchange Membrane Water Electrolysis System[J]. Journal of The Electrochemical Society, 2021.

[24] Ruiz D D H, Sasmito A P, Shamim T. Numerical investigation of the high temperature PEM electrolyzer: effect of flow channel configurations[J]. ECS Transactions, 2013, 58(2): 99.

[25] Toghyani S, Baniasadi E, Afshari E. Numerical simulation and exergoeconomic analysis of a high temperature polymer exchange membrane electrolyzer[J]. International Journal of Hydrogen Energy, 2019, 44(60): 31731-31744.

[26] Suwanwarangkul R, Croiset E, Fowler M W, et al. Performance comparison of Fick's, dusty-gas and Stefan–Maxwell models to predict the concentration overpotential of a SOFC anode[J]. Journal of Power Sources, 2003, 122(1): 9-18.

[27] Kakac S, Pramuanjaroenkij A, Zhou X Y. A review of numerical modeling of solid oxide fuel cells[J]. International journal of hydrogen energy, 2007, 32(7): 761-786.

[28] Xia L, Ni M, He Q, et al. Optimization of gas diffusion layer in high temperature PEMFC with the focuses on thickness and porosity[J]. Applied Energy, 2021, 300: 117357.

[29] Xu H, Chen B, Zhang H, et al. The thermal effect in direct carbon solid oxide fuel cells[J]. Applied Thermal Engineering, 2017, 118: 652-662.

[30] Zhao D, He Q, Yu J, et al. Dynamic behaviour and control strategy of high temperature proton exchange membrane electrolyzer cells (HT-PEMECs) for hydrogen production[J]. International Journal of Hydrogen Energy, 2020, 45(51): 26613-26622.

[31] Luo Y, Shi Y, Li W, et al. Comprehensive modeling of tubular solid oxide electrolysis cell for co-electrolysis of steam and carbon dioxide[J]. Energy, 2014, 70: 420-434.

[32] Torreglosa J P, Jurado F, García P, et al. PEM fuel cell modeling using system identification methods for urban transportation applications[J]. International journal of hydrogen energy, 2011, 36(13): 7628-7640.

[33] Benchouia N E, Derghal A, Mahmah B, et al. An adaptive fuzzy logic controller (AFLC) for PEMFC fuel cell[J]. International Journal of Hydrogen Energy, 2015, 40(39): 13806-13819.

[34] Wu X J, Zhu X J, Cao G Y, et al. Predictive control of SOFC based on a GA-RBF neural network model[J]. Journal of Power Sources, 2008, 179(1): 232-239.

[35] Zhao D, He Q, Wu X, et al. Modeling and optimization of high temperature proton exchange membrane

electrolyzer cells[J]. International Journal of Green Energy, 2021.

A data-driven digital-twin model and control of high temperature proton exchange membrane electrolyzer cells

Dongqi Zhao[a], Qijiao He[b], Jie Yu[b], Meiting Guo[b], Jun Fu[a], Xi Li[a]*, Meng Ni[b]*

a. School of Artificial Intelligence and Automation, Key Laboratory of Image Processing and Intelligent Control of Education Ministry, Huazhong University of Science and Technology, Wuhan, Hubei, China.

b. Department of Building and Real Estate, Research Institute for Sustainable Urban Development (RISUD) and Research Institute for Smart Energy (RISE), The Hong Kong Polytechnic University, Hung Hom, Kowloon, Hong Kong.

*Corresponding author: Xi Li and Meng Ni.

E-mail address: lixi_wh@126.com (Xi Li), meng.ni@polyu.edu.hk (Meng Ni).

Abstract

The high temperature proton exchange membrane electrolyzer cells (HT-PEMEC) are promising for hydrogen generation from fluctuating and intermittent renewable energy. In this study, a data-driven method is developed to study the dynamic behavior of HT-PEMEC. This method combines multiphysics simulation and nonlinear system identification, avoiding expensive experimental costs and time-consuming full multiphysics calculations. Dynamic models for predicting the power consumption, hydrogen production and temperature are identified, and the verified fit is 96.31%, 97.87%, 87.73%, respectively, which demonstrated the accuracy of the identification model. Subsequently, the identification model was used to predict the dynamic behavior of HT-PEMEC and design control strategies. Fuzzy control strategy and neural network predictive control strategy are implemented to alleviate overshoot

and suppress fluctuations so as to improve the durability of the electrolyzer. Moreover, compared with the fuzzy control strategy, the neural network predictive control strategy reduces the power overshoot by approximately 92%. This data-drive digital-twin model can not only guide dynamic experimental research, but also can be extended to study the dynamic behavior of various fuel cells and electrolyzer cells.

Keywords: Proton exchange membrane electrolyzer cell; data-driven method; Numerical modeling; Dynamic research; Control strategy.

Nomenclature

Abbreviation

HT-PEMEC	High temperature proton exchange membrane electrolyzer cell
TPB	Trip phase boundary
FLC	Fuzzy logic control
MPC	Model predictive control
NNPC	Neural network predictive control
GDL	Gas diffusion layer
MSE	Mean square error

Roman

B_0	Permeability coefficient, m^2
E_{act}	Activation energy, $J \cdot mol^{-1}$
C_p	Heat capacity at constant pressure, $J \cdot mol^{-1} \cdot K^{-1}$

D_i^{eff}	Effective diffusivity of species i, $m^2 \cdot s^{-1}$
D_{ik}^{eff}	Knudsen diffusion coefficient of i, $m^2 \cdot s^{-1}$
D_{im}^{eff}	Molecular diffusion coefficient of i, $m^2 \cdot s^{-1}$
i	Operating current density, $A \cdot m^{-2}$
V_{Nernst}	Equilibrium Nernst potential, V
$E_{H_2}^0$	Standard equilibrium potential for hydrogen oxidization, V
F	Faraday constant, 96485 $C \cdot mol^{-1}$
N_i	Flux of mass transport, $kg \cdot m^{-3} \cdot s^{-1}$
i_0	Exchange current density, $A \cdot m^{-2}$
n	Number of electrons transferred per electrochemical reaction
$P_{O_2}^L$	Local O_2 partial pressures, Pa
$P_{H_2}^L$	Local H_2 partial pressures, Pa
$P_{H_2O}^L$	Local H_2O partial pressures, Pa
u	Velocity field, $m^3 \cdot s^{-1}$
R	Gas constant, 8.314 $J \cdot mol^{-1} \cdot K^{-1}$
y_i	Mole fraction of component i
T	Temperature, K

1. Introduction

Sustainable energy conversion and storage technologies are eagerly needed due to the

rapidly increasing energy demand and the significant ecological crisis [1-2]. Moreover, the wide application of intermittent and fluctuating renewable energy, such as photovoltaics and wind energy, requires efficient energy storage technology for reliable power supply [3]. Hydrogen is regarded as an environmentally friendly energy carrier. It can be generated by the electrolysis reaction utilizing excess renewable power, and transformed back to electrical energy by a fuel cell when the electricity supply is insufficient [4-5].

Compared with alkaline water electrolyzer (AWE), proton exchange membrane electrolyzer cell (PEMEC) can generate hydrogen at a higher current density, better dynamic performance and higher hydrogen purity [6-8]. With the development of electrolyte membrane, PEMECs can be operated at a higher temperature of 120 ℃-180 ℃, enabling the use of non-noble metal catalyst [9-10]. Moreover, high temperature PEMEC (HT-PEMEC) can make good use of industrial waste heat for hydrogen production. Compared with solid oxide electrolyzer cells (SOEC) working at 700-800^{o}C, the HT-PEMEC shows the advantage of fast start-up and better durability. Compared with low temperature PEMEC, the electrochemical performance of HT-PEMEC is enhanced due to the high temperature conditions that promote electrode kinetics [11-15]. The increased operating temperature not only reduces the need for electrical energy (reversible voltage), from 1.18 V (80 ℃) to 1.16 V (130 ℃), but also reduces the heat required for electrochemical reactions, from 284 KJ mol^{-1} (80 ℃) to 243 KJ mol^{-1} (130 ℃). Furthermore, water exists as water vapor under high temperature conditions, thus simplifying water management.

Due to its great potential for hydrogen generation, experiments and modeling were

conducted to investigate the dynamic and steady-state performance of HT-PEMEC. Aili et al. [16] developed a polybenzimidazole blend membrane for high temperature steam electrolysis test. The membrane shows lower polarization loss, while the stability is poor at a high current density. Hansen et al. [17] experimentally investigated a phosphoric acid doped perfluorosulfonic acid membrane to improve stability at high temperatures. Compared with conventional perfluorosulfonic acid membranes, the membrane can maintain high stability and conductivity at a high temperature, high current density and acid conditions. Li et al. [18] developed three different flow field modes (cascade, serpentine and parallel) for cathode and anode, and experimentally evaluated the influence of different flow fields on polarization loss. The cathode flow field pattern was found to only impact the ohmic polarization of the electrode, while the anode flow field pattern significantly affected the polarization related to the catalyst layer. Wu et al. [19] experimentally evaluated the influence of operating temperature and pressure on HT-PEMEC. As the temperature and pressure increase, the current density of oxygen evolution increases, while the terminal voltage decreases. Garbe et al. [20] studied the effect of operating temperature on the overpotential loss. The experimental results show that activation loss is the main overpotential loss at high temperatures. Li et al. [21] experimentally explored the influence of operating conditions on the voltage of HT-PEMEC. It was found that increasing temperature under the pressure of 0.1 MPa increased the concentration loss but the ohmic loss remained unchanged, and the overpotential loss caused by the temperature change could be suppressed by adjusting the pressure. Natarajan et al. [22] experimentally explored the effect of different calcination temperatures on high-temperature electrolysis performance.

The PEMEC calcined at 500 ℃ achieved the best performance.

Apart from experimental studies, several modeling studies were conducted on HT-PEMEC. The models for PEMEC can be classified into groups: analytical models, semi-empirical models and computational fluid dynamics (CFD) models. Among them, CFD models are widely used due to their strong interpretability and accuracy. Tijani et al. [23] built a 3D CFD model to optimize the bipolar plate of PEMEC. The optimized parallel flow field design can reduce both the pressure drop and the internal turbulence significantly. Ruiz et al. [24] built a CFD model to investigate the effects of three different flow channel configurations (serpentine, multiple serpentine and parallel) on the performance of the electrolytic cell. The results show that the multiple-serpentine flow channel has better performance in terms of temperature uniformity and hydrogen generation. Zhang et al. [25] developed a numerical model to evaluate the influence of the flow channel configuration on the electrolyzer cell. Compared with the co-flow mode, the counter-flow mode has a lower temperature and a greater temperature gradient. Jia et al. [26] developed a multiphysics model to study the dynamic behavior of oxygen in the electrolyzer manifold. It turns out that the pressure and gas velocity take about 2 seconds to stabilize, and the oxygen production rate and pressure drop can be adjusted by the number of channels. S.Toghyani et al. [27] proposed a finite element numerical simulation model to investigate the influence of operating conditions and structural parameters of HT-PEMEC on electrochemical performance. Scheepers et al. [28] investigated the effect of temperature optimization on the overall electrolysis process. The optimal temperature depends on the electrode pressure and operating voltage, and hydrogen permeation is significantly

alleviated by optimizing the temperature at low current densities. Bonanno et al. [29] evaluated the energy efficiency and exergy efficiency of PEMEC from a system perspective. The high system efficiency was attributed to the high heat utilization rate under thermally neutral conditions. Toghyani et al. [30] proposed a non-isothermal model based on the finite volume method for efficiency and exergoeconomic analysis. The higher temperature was found to reduce the cost of the HT-PEMEC and increase the exergy efficiency, and the high-pressure operating condition also promotes cost reduction.

Based on the above literature survey, it is clear that the current research focuses on the influence of operating conditions and structural parameters on the performance of HT-PEMEC, while the dynamic behavior is rarely studied. The rapid electrochemical reaction and relatively slow mass transfer easily cause overshoot and fluctuations in the dynamic behavior, which leads to a decrease in system durability. Therefore, the research of dynamic processes is necessary. As shown in Fig. 1a, experimental testing is very time-consuming, expensive, and cannot provide detailed information in the electrolyzer cell. Multiphysics modeling can provide detailed information but it is computationally demanding. The method of combining the multiphysics model with system identification is thus proposed to study the dynamic process of the nonlinear dynamic system to achieve both high accuracy and low computational cost. The dynamic research framework is presented in Fig. 1b. The multiphysics model was developed and validated to investigate the performance of HT-PEMEC. Datasets of dynamic behavior are generated by adjusting the input of the multiphysics model. Then, the datasets are used for system identification. After the identification model is verified by comparison with

the multiphysics model, which is used to design control strategies. This method can also be extended to other dynamic studies of fuel cells and electrolyzer cells.

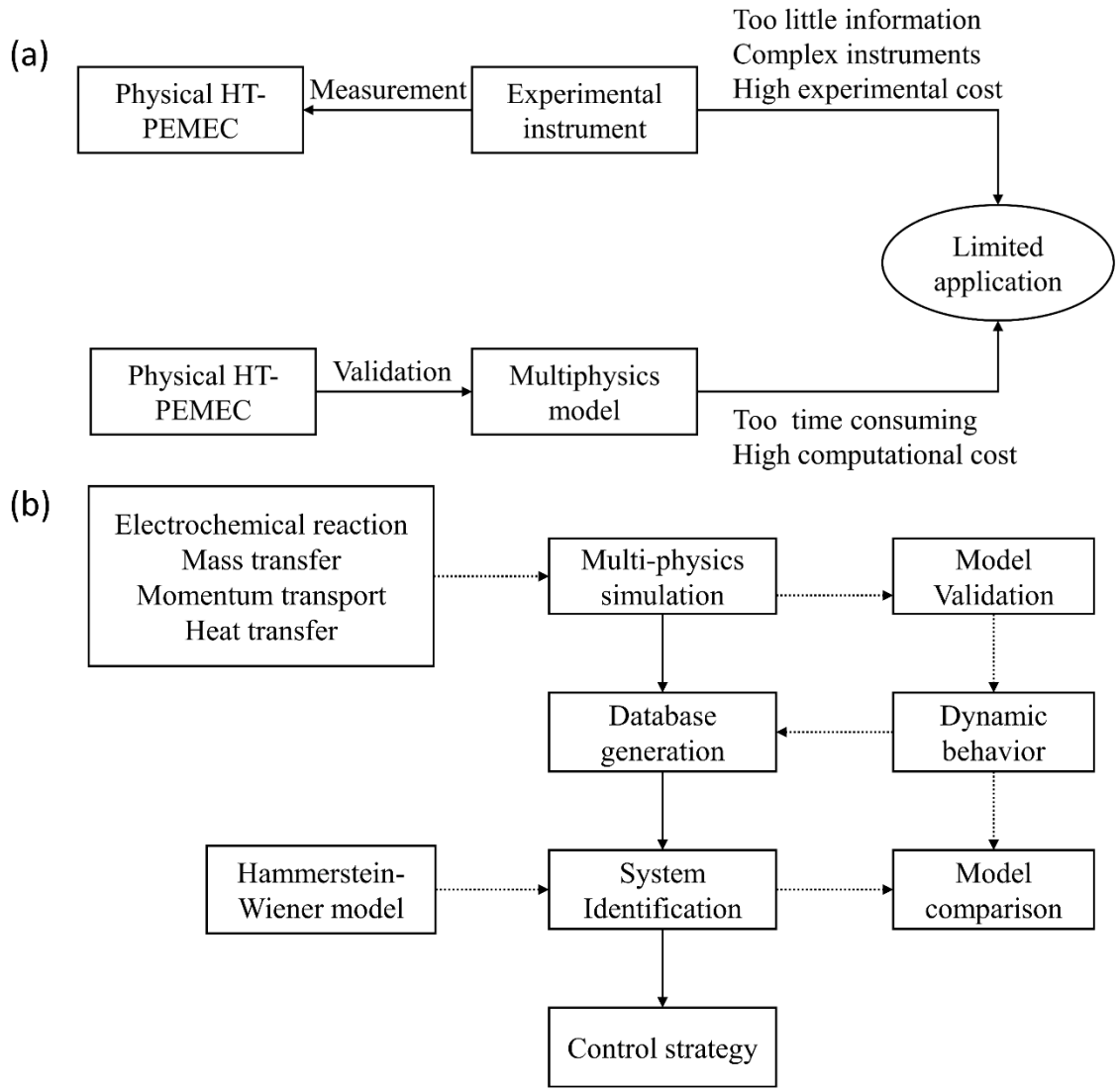

Fig. 1. (a) The application limitations of experimental observation and multiphysics model; (b) Data-driven dynamic research framework.

2. Multi-physics model development

The two-dimensional multiphysics model has been developed to explore the dynamic processes, including electrochemical reaction, temperature distribution, mass/momentum

transportation and electron/ion conduction [35]. The schematic diagram of HT-PEMEC is shown in Fig. 2. It is noted that no microporous layer (MPL) is used in HT-PEMEC. MPL is usually used in low temperature PEMFC for removing liquid water, while water is in the form of vapor in HT-PEMEC, thus it is not needed. In operation, steam is introduced into the cathode and anode, while steam at the cathode side only serves as a carrier gas. Gaseous H_2O molecules transport through the porous anode to TPB, generating oxygen, hydrogen protons and electrons. Hydrogen protons diffuse through the membrane to the catalytic layer of the cathode, and combine with electrons to produce hydrogen molecules. The detailed model parameters are listed in Table 1.

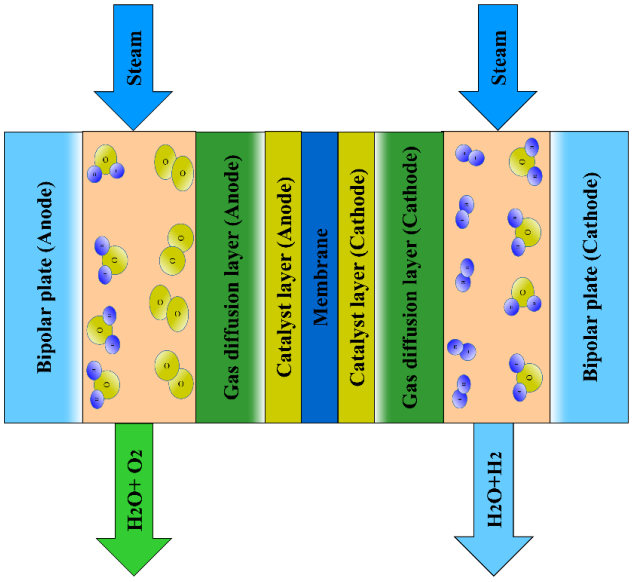

Fig.2. Schematic figure of the HT-PEMEC.

Table 1. Physical and geometric parameters of the model.

Parameter	value	unit
Channel height	1	mm
Channel length	50	mm
Channel width	1	mm
Membrane thickness	0.1	mm
Catalyst layer thickness	0.05	mm

Gas diffusion layer thickness	0.38	mm
Operating temperature	403.15	K
Operating pressure	1	bar
Porosity of catalyst layer	0.3 [25]	
GDL porosity	0.4 [25]	
Catalyst layer permeability	2.36×10^{-12} [41]	m^2
GDL permeability	1.18×10^{-11} [41]	m^2
Anode exchange current density	10^{-4} [42]	A cm^{-2}
Cathode exchange current density	0.1 [42]	A cm^{-2}
Anode gas flow rate	0.2	m s^{-1}
Cathode gas flow rate	0.2	m s^{-1}
Proton conductivity of electrolyte	20 [43]	S m^{-1}

2.1 Model assumption

The following assumptions are utilized in the finite element method.

(1) All porous materials are isotropic and homogeneous;

(2) All gases (H_2O, H_2, O_2) in the multi-physics model are regarded as ideal gases;

(3) TPB is evenly distributed in the porous catalyst layer.

2.2 Electrochemical reaction

In this model, the electrolysis reaction of the anode and cathode is written as Eq. (1) and (2).

$$\text{Anode: } 2H_2O \rightarrow O_2 + 4H^+ + 4e^- \quad (1)$$

$$\text{Cathode: } 2H^+ + 2e^- \rightarrow H_2 \quad (2)$$

The equilibrium potential of the electrochemical reaction can be calculated as follows.

$$V_{Nernst} = E^0_{H_2} + \frac{RT}{2F} ln\left[\frac{P^L_{H_2}\left(P^L_{O_2}\right)^{1/2}}{P^L_{H_2O}}\right] \quad (3)$$

Here $E^0_{H_2}$ represents the standard potential of the electrochemical reaction. $P^L_{H_2}$, $P^L_{H_2O}$ and

$P_{O_2}^{L}$ represent the local pressure of various gases. Moreover, the local gas partial pressure at TPB is used, thereby the concentration loss is incorporated in the equilibrium potential Eq. (3).

The operating voltage applied to the electrodes of the electrolyzer is expressed as Eq. (4).

$$V_{cell} = V_{Nernst} + \eta_{act} + \eta_{ohm} \tag{4}$$

Activation overpotential (η_{act}) represents the energy barrier of the electrolysis reaction on the porous electrode, which is mainly related to the electrode material and microstructure. The activation overpotential can be expressed by the Buttler-Volmer equation.

$$\mathrm{i} = i_0 \left\{ exp\left(\frac{\alpha n F \eta_{act}}{RT}\right) - exp\left(\frac{(1-\alpha) n F \eta_{act}}{RT}\right) \right\} \tag{3}$$

$$i_0 = \gamma \exp(-\frac{E_{act}}{RT}) \tag{4}$$

Here α represents the transfer coefficient, n represents the number of transferred electrons, E_{act} denotes the activation energy of the electrochemical reaction, γ denotes the pre-exponential factor of Eq. (4).

The ohmic overpotential (η_{ohm}) is caused by the resistance of proton and electron transport in the electrolyzer, which usually is expressed by the Ohm law.

2.3 Fluid flow and mass transport

The mass transport of various gases in porous media and channels is described by Eq. (5) and Eq. (6) [31].

$$N_i = -\frac{1}{RT}\left(\frac{B_0 y_i P}{\mu}\nabla P - D_i^{eff}\nabla(y_i P)\right) \text{ (i=1,2,…..n)} \tag{5}$$

$$D_i^{eff} = \frac{\varepsilon}{\tau}\left(\frac{1}{D_{im}^{eff}} + \frac{1}{D_{ik}^{eff}}\right) \tag{6}$$

Here N_i represents the mass transfer flux of component i, y_i represents the molar

fraction of i, B_0 represents permeability coefficient, μ is gas viscosity, τ is tortuosity, ε is porosity. Furthermore, the mass conservation is expressed as Eq. (7).

$$\nabla\left(-D_i^{eff}\nabla C_i\right) = R_i \tag{7}$$

Here C_i and R_i are the mole concentration and the mass source term of component i, respectively.

Navier-Stokes equation is utilized to calculate the momentum transfer in porous media and channels [32].

$$\rho\frac{\partial \mathrm{u}}{\partial \mathrm{t}} + \rho \mathrm{u}\nabla \mathrm{u} = -\nabla \mathrm{p} + \nabla\left[\mu(\nabla \mathrm{u} + (\nabla \mathrm{u})^T) - \frac{2}{3}\mu\nabla \mathrm{u}\right] - \frac{\varepsilon\mu \mathrm{u}}{B_0} \tag{8}$$

Here u and ρ are the velocity vector and gas density. Table 2 lists the physical parameters of various gases.

Table 2. Physical properties of gaseous components [33,44].

Parameter	Value
Viscosity of H_2O	$(-36.826+4.29e^{-1}\cdot T-1.62\ e^{-5}\cdot T^2)\cdot 1e^{-7}$ [Pa•s]
Viscosity of H_2	$(27.758+2.12e^{-1}\cdot T-3.28e^{-5}\cdot T^2)\cdot 1e^{-7}$ [Pa•s]
Viscosity of O_2	$(44.224+5.62e^{-1}\cdot T-1.13e^{-5}*T^2)\cdot 1e^{-7}$ [Pa•s]
Heat capacities of H_2O	$33.93-8.42e^{-2}\cdot T+2.99e^{-5}\cdot T^2-1.78e^{-8}\cdot T^3+ 3.69e^{-12}\cdot T^4$ [J•mol^{-1}•K^{-1}]
Heat capacities of H_2	$25.4+2.02e^{-2}\cdot T-3.85e^{-5}\cdot T^2+3.19e^{-8}\cdot T^3-8.76e^{-12}\cdot T^4$ [J•mol^{-1}•K^{-1}]
Heat capacities of O_2	$29.53-8.90e^{-2}\cdot T+3.81e^{-5}\cdot T^2-3.26e^{-8}\cdot T^3+ 8.86\cdot e^{-12}*T^4$ [J•mol^{-1}•K^{-1}]

Thermal conductivities of H_2O	$0.53e^{-3}+4.71e^{-4}\bullet T+4.96e^{-8}\bullet T^2$ [$W\bullet m^{-1}\bullet K^{-1}$]
Thermal conductivities of H_2	$0.36e^{-1}+4.59e^{-4}\bullet T-6.49e^{-8}\bullet T^2$ [$W\bullet m^{-1}\bullet K^{-1}$]
Thermal conductivities of O_2	$0.12e^{-2}+8.62e^{-4}\bullet T-1.33e^{-8}\bullet T^2$ [$W\bullet m^{-1}\bullet K^{-1}$]

2.4 Temperature field model

The electrochemical reaction is endothermic but the overpotential loss is exothermic, and the temperature distribution can be calculated by the heat balance equation as Eq. (8) and Eq. (9) [34].

$$\rho C_p u \bullet \nabla T + \nabla\left(-\lambda_{eff}\nabla T\right) = Q \tag{8}$$

$$\lambda_{eff} = (1-\varepsilon)\lambda_s + \varepsilon\lambda_g \tag{9}$$

Here C_p is the fluid heat capacity, u is the flow rate, λ_{eff} is the effective thermal conductivity, λ_s represents the solid thermal conductivity, λ_g represents gaseous thermal conductivity. Q represents heat source, including heat generation (Q_{Gen}) due to overpotential loss and heat consumption (Q_{Con}) due to electrolysis reaction.

$$\begin{cases} Q_{Gen} = E_{Irr} \times \mathrm{i} \\ Q_{Con} = T\Delta S = \Delta H - \Delta G \end{cases} \tag{10}$$

Here E_{Irr} is overpotential, ΔS and ΔH are the entropy change and reaction enthalpy, ΔG represents the Gibbs free energy.

2.5 Boundary conditions and validation

Both the cathode and anode of HT-PEMEC are open-end. The operating voltage is applied to the outer surfaces of the anode and cathode. Back gas pressure is specified as 1 atm. The

operating temperature and flow rate of the anode and cathode inlets are specified. The walls are adiabatic. The time step of the dynamic solver is set to 0.01s. The multiphysics model was solved utilizing the finite element method. More details about the model and the model validation can be found in ref. [35, 40].

3. Dynamic system identification

Multiphysics model can provide more accurate results than analytical models and semi-experimental models, thus it is widely used to analyze the dynamic and steady-state behavior of electrolyzer cells and fuel cells. However, the calculation process of the multiphysics model is time-consuming, thereby it is not suitable for real-time control purposes. Transfer functions or state equations are obtained which are necessary for complex control strategies, such as robust control and predictive control. The transfer functions identified from the multiphysics model are a very efficient method. It not only ensures the accuracy of the model but also improves computational efficiency.

The measured data is required to adequately reflect the dynamic behavior of the system to identify an accurate model. Therefore, the dynamic behavior between random non-periodic steady-state operating points is measured, and the time interval of the step response allows the dynamic process to reach a steady-state to obtain a time constant. Fig. 3 shows the identification and validation data obtained from the multiphysics model. Identification data and validation data are collected by adjusting the operating voltage, and the anode flow rate was sufficiently large to suppress reactant starvation during the dynamic process. The data is acquired with a sampling interval of 0.01 s and a duration of 1200 s. Furthermore, two sets of dynamic data are

obtained from the multiphysics model, one set of data is used to identify the transfer functions model, and the other set of data is used for validation.

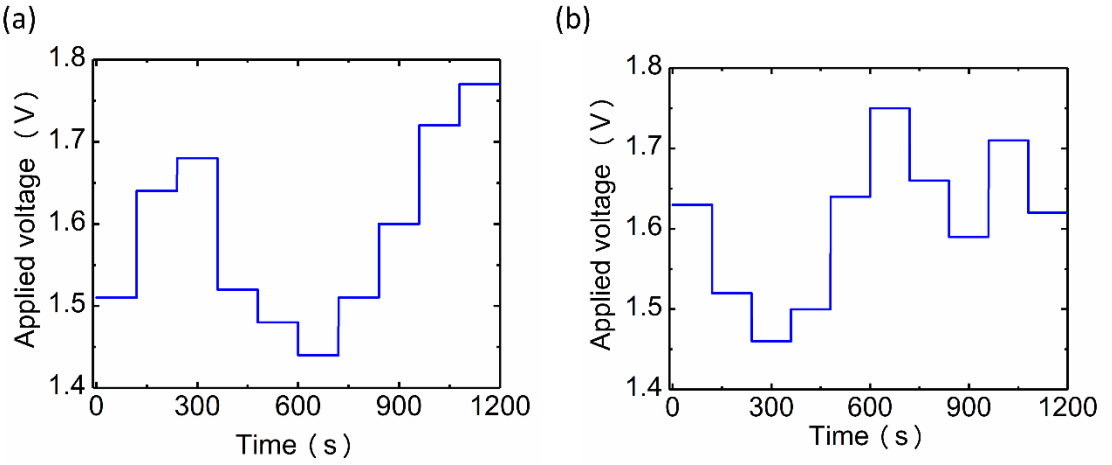

Fig. 3. (a) The voltage adjustment in identification data; (b) The voltage regulation in validation data.

The transfer function model was identified from the identification data using System Identification Toolbox™ of Matlab. The research focuses on identifying the dynamic behavior of the electrolyzer cell without considering a specific mathematical structure, hence the black-box identification technique is chosen. However, black-box modeling is generally an error-and-trial process, thus the structure and parameters of the model are estimated and compared to optimize model accuracy. System identification usually starts with a linear structural model and attempts to use higher order models or non-linear structures when the fit is poor. The method of system identification is regarded as a single-input single-output (SISO) model to reduce the coupling between different sub-models to improve identification accuracy. The power consumption sub-model, the hydrogen generation sub-model and the temperature sub-model were developed to study the control strategy in the dynamic process and calculate the

electrolysis efficiency.

The efficiency of an HT-PEMEC can be determined as a ratio of input energy to output energy. The input energy includes the input electrical energy and the input thermal energy for heating gas, and the output energy is the chemical energy produced [36].

$$\eta = \frac{(\dot{m}_{o,H_2} - \dot{m}_{i,H_2}) LHV_{H_2}}{V \int_0^{L_{RU}} i dz + \dot{m}_{i,ca} \int_{T_0}^{T_{i,ca}} C_{p,g,ca} dT + \dot{m}_{i,an} \int_{T_0}^{T_{i,an}} C_{p,g,an} dT} \tag{11}$$

Where $\dot{m}_{i,H_2}$ and $\dot{m}_{o,H_2}$ are hydrogen mass flow rate at inlet and outlet. $\dot{m}_{i,ca}$ and $\dot{m}_{i,an}$ denote the cathode and anode gas mass flow rates, respectively. $C_{p,g,ca}$ and $C_{p,g,an}$ represent the cathode and anode gas heat capacities.

3.1 Identification results

The structure and order of the linear model are obtained by trial and error, and the general output-error (OE) model is represented as Eq. (12) [37].

$$\mathrm{y(t)} = \frac{B(z)}{F(z)} u(t-n) + e(t) \tag{12}$$

Here u(t) denotes system input, y(t) denotes the system output, e(t) denotes system disturbance, n indicates system delay. F(z) and B(z) are polynomials with regard to the z^{-1} operator, respectively.

$$\begin{cases} B(z) = b_0 + b_1 z^{-1} + b_2 z^{-2} + \cdots + b_{kb-1} z^{-(kb-1)} \\ F(z) = 1 + f_1 z^{-1} + f_2 z^{-2} + \cdots + f_{kf} z^{-kf} \end{cases} \tag{13}$$

HT-PEMEC is a non-linear system and therefore non-linear factors need to be added to the linear model. Hammerstein-Wiener models are generally used to describe the dynamic behavior of non-linear systems. As shown in Fig. 4, the Hammerstein-Wiener model consists

of a linear block, an input nonlinearity and an output nonlinearity. The linear block is used to describe the dynamics of the modeled system, while the input nonlinearity and output nonlinearity are used to reflect the nonlinear characteristics of the system.

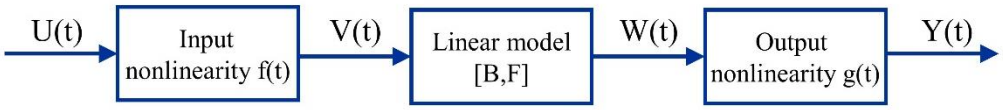

Fig. 4. Hammerstein-Wiener model framework

The accuracy of the fit can be described as Eq. (14).

$$\text{Fit} = \left(1 - \frac{\|y-\hat{y}\|}{\|y-\hat{y}\|}\right) \times 100\% \tag{14}$$

Here y represents the output of multiphysics data, $\hat{y}$ denotes the output of the identification model. $\bar{y}$ denotes the average of y.

The mean squared error (MSE) is also used to validate the model and is expressed as Eq. (15).

$$\text{MSE} = \frac{1}{N}\sum_{j=1}^{N}(y-\hat{y})^2 \tag{15}$$

Here N denotes the total number of data, and j represents the jth output result.

3.1.1 Applied voltage versus power consumption sub-model

System dynamics are first obtained by identifying linear systems to determine the coefficients of B and F. Subsequently, the best performance was observed by describing the input nonlinearity and the output nonlinearity using segmented functions and one-dimensional polynomials respectively. The voltage versus power consumption sub-model can be expressed as Eq. (16).

$$\begin{cases} f(t) = \begin{cases} 2.54u(t) - 3.849\ 0 \ll u(t) < 1.65 \\ 4.065u(t) - 6.367\ u(t) \geq 1.65 \end{cases} \\ \begin{cases} w(t) = \left[\frac{\mathrm{B(z)}}{\mathrm{F(z)}}\right] v(t) + e(t) \\ \mathrm{B(z)} = z^{-1} - 0.9918z^{-2} \\ \mathrm{F(z)} = 1 - 0.9372z^{-1} - 0.0077z^{-2} - 0.0452z^{-3} \end{cases} \\ g(t) = 5.1478E^3 w(t)^2 + 2.2109E^3 w(t) + 315.6857 \end{cases} \tag{16}$$

Here u(t) is applied voltage, y(t) is power density (W m^{-2}). Fig. 5 shows the results of the identification and validation data compared to the output of the identification model. The power consumption sub-model is able to describe the system dynamics and the corresponding evaluation indicators are listed in Table 3.

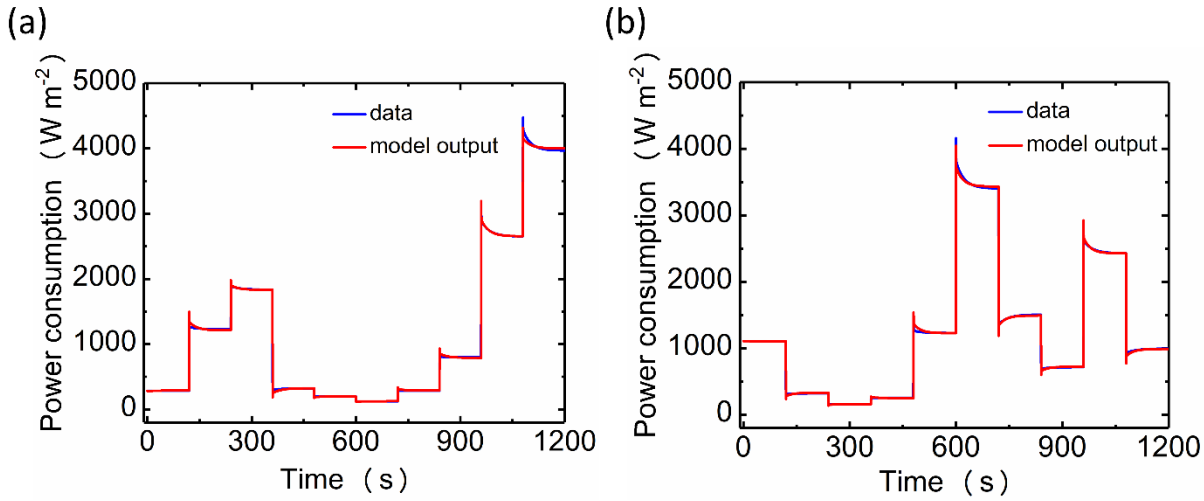

Fig. 5. (a) Comparison of identification model output and identification data; (b) Comparison of identification model output and validation data.

3.1.2 Applied voltage versus hydrogen generation sub-model

The hydrogen generation sub-model has a similar structure to the power consumption sub-model because the hydrogen generated is proportional to the current density. Therefore, the best performance is obtained by selecting the piecewise function to describe the input

nonlinearity and the one-dimensional polynomial to describe the output nonlinearity, respectively. The voltage versus hydrogen generation sub-model can be expressed as Eq. (17).

$$\begin{cases} f(t) = \begin{cases} 1.448u(t) - 2.197\ 0 \ll u(t) < 1.62 \\ 1.966u(t) - 3.035\ u(t) \geq 1.62 \end{cases} \\ \begin{cases} w(t) = \left[\frac{\mathrm{B(z)}}{\mathrm{F(z)}}\right] v(t) + e(t) \\ \mathrm{B(z)} = z^{-1} - 0.9926z^{-2} \\ \mathrm{F(z)} = 1 - 1.17183z^{-1} + 0.8562z^{-2} - 0.1345z^{-3} \end{cases} \\ g(t) = 1.7556E^{-4}w(t)^2 + 1.1739E^{-4}w(t) + 3.1594E^{-5} \end{cases} \quad (17)$$

Here u(t) is applied voltage, y(t) is hydrogen generated (kg m^{-2} s^{-1}). As shown in Fig. 6, the identification model output is compared with the identification and validation data to verify the hydrogen generation sub-model. Furthermore, the performance indicators are summarized in Table 3.

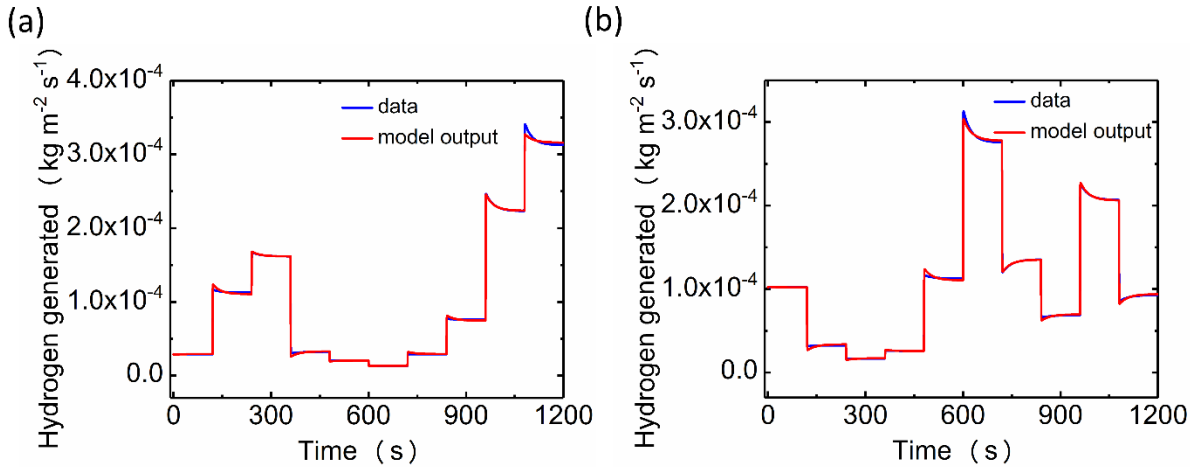

Fig. 6. (a) Comparison of identification model output and identification data; (b) Comparison of identification model output and validation data.

3.1.3 Applied voltage versus temperature sub-model

Heat transfer is relatively slow compared to the dynamics of other physical parameters and the thermal model has high delays and strong non-linearity. The best performance of the

identification model was observed through the use of segmentation functions and one-dimensional polynomials to describe input nonlinearity and output nonlinearity. The voltage versus temperature sub-model can be expressed as Eq. (18).

$$\begin{cases} f(t) = \begin{cases} 0.1296u(t) - 0.2225 \; 0 \ll u(t) < 1.61 \\ 0.5676u(t) - 0.9277 \; u(t) \geq 1.61 \end{cases} \\ \begin{cases} w(t) = \left[\frac{\mathrm{B(z)}}{\mathrm{F(z)}}\right] v(t) + e(t) \\ \mathrm{B(z)} = -0.422z^{-1} + z^{-2} - 0.4538z^{-3} - 0.7063z^{-4} + 0.8802z^{-5} - 0.2982z^{-6} \\ \mathrm{F(z)} = 1 - 3.1524z^{-1} + 3.0392z^{-2} + 0.6171z^{-3} - 3.3842z^{-4} + 2.5233z^{-5} - 0.643z^{-6} \end{cases} \\ g(t) = 29.7651w(t)^2 - 17.5995w(t) + 414.9453 \end{cases}$$

(18)

Here u(t) is applied voltage, y(t) denotes operating temperature (K). Fig. 7 shows the comparison of the identification and validation data with the model output. The temperature identification model has a lower fit compared to the power consumption sub-model and the hydrogen generated sub-model, due to the high delays and strong non-linearity of the temperature model. However, the errors are acceptable and the corresponding evaluation indicators are listed in Table 3.

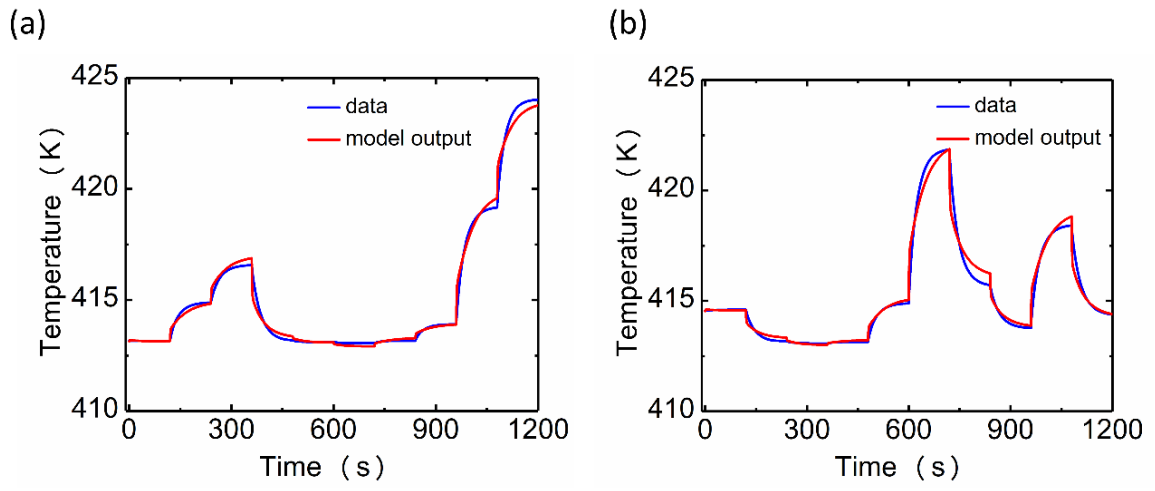

Fig. 7. (a) Comparison of identification model output and identification data; (b)

Comparison of identification model output and validation data

Table 3. Identification model evaluation index.

Indicator	Power consumption sub-model		Hydrogen generated sub-model		Temperature sub-model	
	Identification data	Validation data	Identification data	Validation data	Identification data	Validation data
Fit (%)	97.57	96.31	98.1	97.87	92.66	87.73
MSE	0.913	1.352	$6.253E^{-12}$	$9.918\ E^{-12}$	0.1011	0.2295

4. Dynamic control strategy

The utilization of excess renewable energy to produce hydrogen for subsequent fuel cells and industrial applications is the most promising pathway for HT-PEMEC. However, the fast electrochemical response easily triggers excessive overshoot and fluctuation, resulting in poor durability and dynamic performance. Therefore, dynamic research is necessary for long-term stable operation. Dynamic multi-physics models can be used to analyze the dynamic behavior of electrolyzer cells to develop control strategies. Subsequently, the performance of the control strategy can be verified in the identified dynamic system to provide a reference for the experiment.

4.1 Dynamic behavior

The dynamic process of HT-PEMEC can be divided into two stages, namely, rapid electrochemical response and relatively slow mass transfer process. As shown in Fig. 8, the transient process of the operating voltage from 1.6 V to 1.7 V.

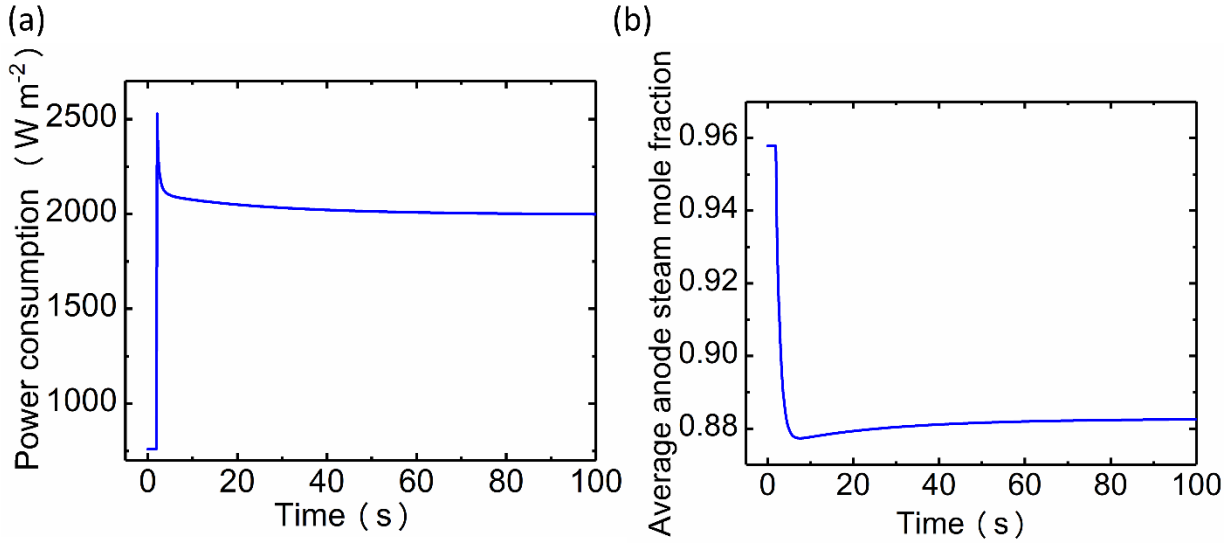

Fig. 8. (a) Dynamic response of power consumption; (b) Dynamic response of steam mole fraction in the catalytic layer.

An obvious overshoot exists in the dynamic process of power response. The power consumption rises rapidly due to the fast electrochemical response, however, the relatively slow mass transfer process leads to a rapid decrease in the reactant concentration, which eventually causes the power consumption to drop to a steady-state. To alleviate overshoot and fluctuation, it is essential that the electrochemical response be adjusted during the dynamic process.

4.2 Fuzzy logic control strategy

Fuzzy logic control (FLC) strategy is a rule-based nonlinear control method. Moreover,

the main advantage of the method can be applied to dynamic systems where models are difficult to obtain, and inference rules can be designed based on the experience of human experts [38]. The 2D FLC can adjust the control strategy according to the error and the change of the error in real time, and its work flow is shown in Fig. 9. The fuzzification process uses membership functions to convert precise input into fuzzy language, and then calculates the output through pre-set inference rules, lastly, the output is converted into precise control parameters by defuzzification.

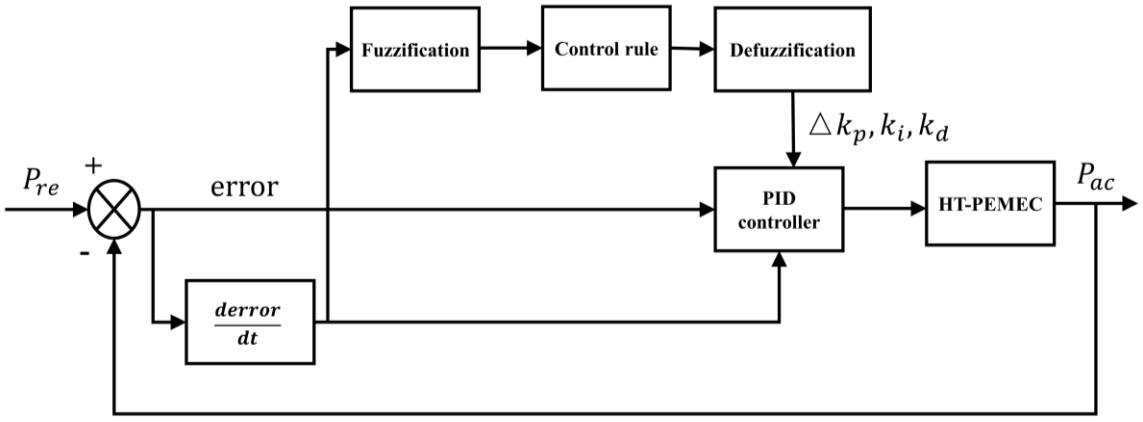

Fig. 9. The 2D fuzzy logic controller framework

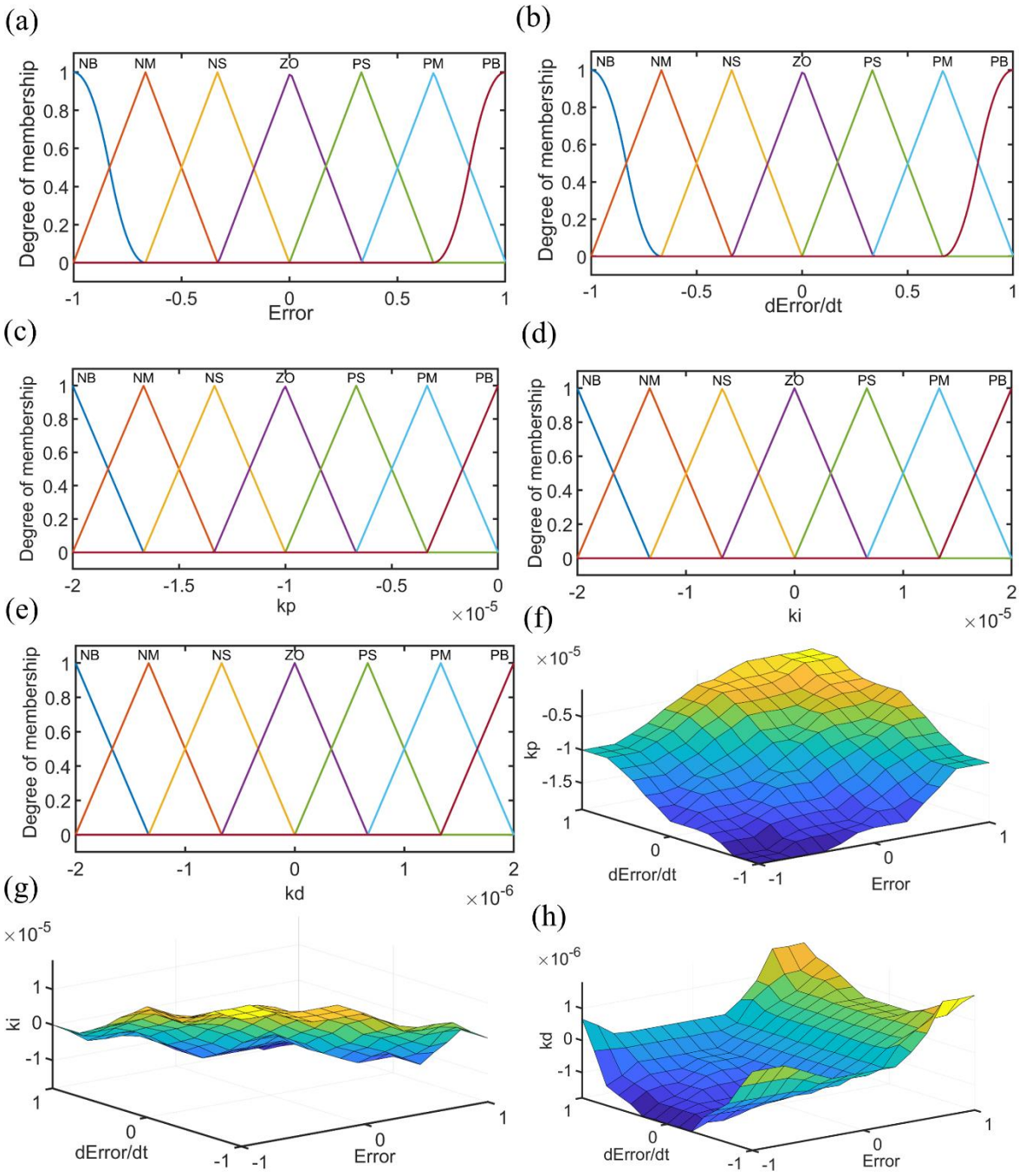

Fig. 10. (a) Membership function of the error; (b) Membership function of the change of error; (c) Membership function of the change of k_p; (d) Membership function of the change of k_i; (e) Membership function of the change of k_d; (f) Output characteristic of the change of k_p; (g) Output characteristic of the change of k_i; (h) Output characteristic of the change of k_d;

Here P_{re} is the reference power, P_{ac} is the actual power density. Δk_p, Δk_d and Δk_i are the changes in the control coefficients respectively. This fuzzy logic block has three outputs and two inputs; the inputs represent the error and the change of error, and the outputs are the changes in k_p, k_d and k_i respectively. The fuzzy subsets of output and input are divided into {NB, NM, NS, ZO, PS, PM, PB}. Moreover, the output characteristics and membership function are shown in Fig. 10. The fuzzy logic control strategy is applied as the control signal is initially enhanced to accelerate the dynamic response and subsequently reduced to suppress overshoot.

4.3 Neural Network Predictive Control Strategy

Model predictive control is a nonlinear control strategy based on model prediction and online optimization. Moreover, model predictive control has a wider control horizon due to the ability to predict dynamic behavior compared to other control strategies [39]. The neural network predictive control (NNPC) strategy uses a non-linear neural network to predict the dynamic behavior of the HT-PEMEC, thereby optimizing the dynamic behavior to reduce overshoot. The detailed workflow of NNPC is shown in Fig. 11 and specific implementation steps can refer to the Deep Learning Toolbox of Matlab.

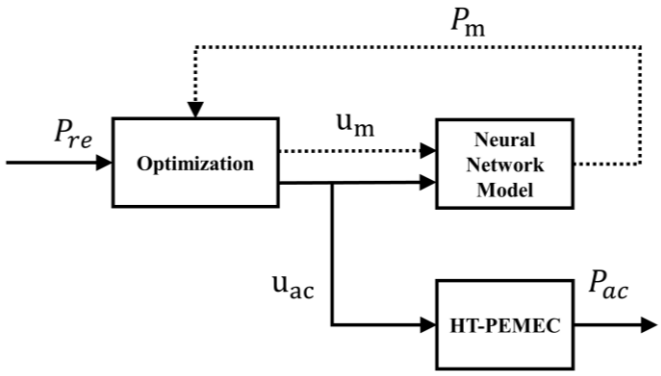

Fig. 11. The Neural network predictive control framework

Here P_m is the predictive model output, u_m is the predictive model input and u_{ac} is the actual electrolyzer input. The optimization is implemented through the calculation of Eq. 20, and then the optimized input voltage u_{ac} is supplied to the electrolyzer to optimize the dynamic process.

$$J = \sum_{j=1}^{N_p}[P_{re}(k+j) - P_m(k+j)]^2 + \rho \sum_{j=1}^{N_c}[u_m(k+j-1) - u_m(k+j-2)]^2 \quad (20)$$

Here N_c represents the control time domain length, N_p represents the predicted time domain length and ρ is the weighting factor. Optimization is performed by calculating the minimum value of J. NNPC adjusts the operating voltage by predicting the dynamic behavior of HT-PEMEC to alleviate overshoot and fluctuation.

4.4 Results and analysis

Fuzzy logic control strategy and neural network predictive control strategy are applied in the dynamic process of HT-PEMEC to suppress overshoot and fluctuation. The random variation of power consumption is used to represent renewable energy, with an interval of 30 seconds and a sampling interval of 0.01s. Furthermore, the dynamic response and control

strategy of the electrolyzer were compared, as shown in Fig. 12.

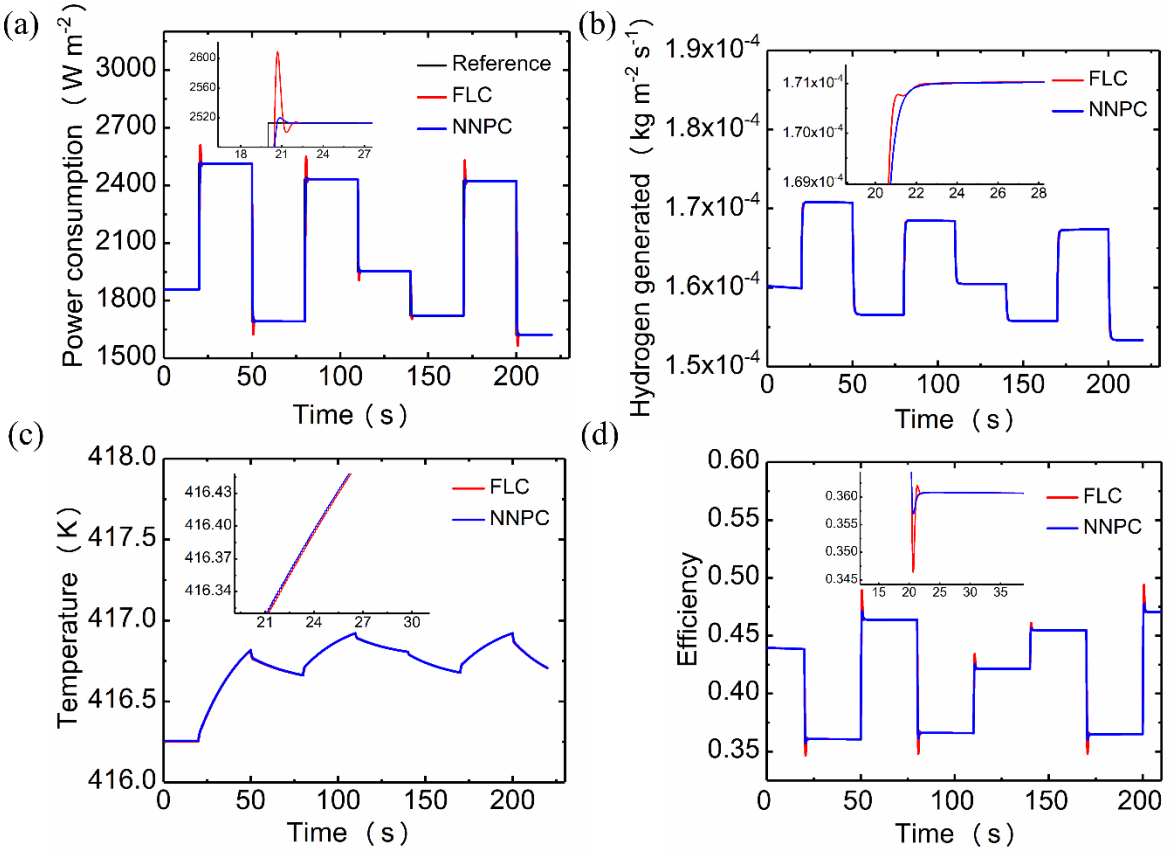

Fig.12. (a) Dynamic response of power consumption; (b) Dynamic response of hydrogen generated; (c) Dynamic response of temperature; (d) Efficiency changes in dynamic processes.

The dynamic behavior of energy consumption is shown in Fig. 12a. Neural network predictive control strategy shows better dynamic performance and smaller overshoot compared to the fuzzy logic control strategy. For instance, in a random step from 1857 W m^{-2} to 2513 W m^{-2}, the power overshoot of the neural network predictive control strategy is reduced by 92% compared to the fuzzy logic control strategy. Furthermore, neural network predictive control can predict the dynamic behavior of HT-PEMEC for online optimization, compared with the fuzzy logic control strategy optimized based on real-time error and error change rate, it has a

wider control horizon to reduce the overshoot. The fuzzy logic control strategy calculates the controller output according to the pre-made fuzzy inference rules, which requires fewer calculation resources than the neural network predictive control strategy. The hydrogen generation rate in the dynamic process is shown in Fig. 12b. Furthermore, the hydrogen production rate under the fuzzy logic control strategy is greater than the neural network predictive control strategy due to the dramatic power consumption increase and excessive overshoot in the initial phase of the dynamic process, the subsequent two control strategies maintain the same hydrogen production rate. The temperature response of neural network predictive control is similar to the fuzzy logic control strategy, and the results are shown in Fig. 12c. The dynamic efficiency calculation can be divided into the input electric energy, the heating gas energy, and the chemical energy produced. As shown in Fig. 12b and Fig. 12c, There is little difference between the energy of heating gas and the chemical energy produced in the dynamic process, thus the fluctuation of efficiency is mainly affected by the input electrical energy. It can be observed from Fig. 12d that the fluctuation of the efficiency during the dynamic process corresponds to the overshoot of the power consumption. Overall, neural network predictive control strategies can provide better dynamic performance.

Conclusions

Traditional experimental observations require complex instruments and high experimental costs to study the dynamic process of HT-PEMEC. Moreover, the widely used multiphysics

model is time-consuming and requires a lot of computing resources. The data-driven dynamic research method is proposed to simplify the research process by combining multiphysics models and system identification methods, which can achieve fast computation with sufficient accuracy. A 2D multiphysics simulation model was established to study the electrolyzer cell, in which electrochemistry, mass transfer, momentum transfer and heat transfer were considered. Subsequently, the dynamic data generated by the multiphysics model is used for system identification. Furthermore, The identification model is verified by comparison with the multiphysics model.

To predict the dynamic behavior of HT-PEMEC and calculate the efficiency in the dynamic process, the power consumption sub-model, the hydrogen generation sub-model and the operating temperature sub-model are identified. Fuzzy logic control strategy and neural network predictive control strategy are designed to control power consumption to improve dynamic behavior. Neural network predictive control shows better dynamic performance and smaller overshoot compared to fuzzy logic control strategies, but it requires more computing resources. In a random step from 1857 W m^{-2} to 2513 W m^{-2}, the power overshoot of the neural network predictive control strategy is reduced by 92% compared to the fuzzy logic control strategy.

This data-driven approach provides a promising solution by combining multiphysics models and system identification, which can quickly and accurately analyze the performance of nonlinear dynamic systems. Currently, this method is only used in the single-input single-output system, and then can be applied to a multiple-input multiple-output system and consider

the coordinated control of multiple physical parameters.

Acknowledgments

M. NI thanks the grants (Project Number: PolyU 152064/18E and N_PolyU552/20) from Research Grant Council, University Grants Committee, Hong Kong SAR.

References

[1] Luo X, Wang J, Dooner M, et al. Overview of current development in electrical energy storage technologies and the application potential in power system operation[J]. Applied energy, 2015, 137: 511-536.

[2] Su Y W. Residential electricity demand in Taiwan: Consumption behavior and rebound effect[J]. Energy Policy, 2019, 124: 36-45.

[3] Dincer I. Renewable energy and sustainable development: a crucial review[J]. Renewable and sustainable energy reviews, 2000, 4(2): 157-175.

[4] Tarhan C, Çil M A. A study on hydrogen, the clean energy of the future: Hydrogen storage methods[J]. Journal of Energy Storage, 2021, 40: 102676.

[5] Dafedar A A, Verma S S, Yadav A. Hydrogen Storage Techniques for Stationary and Mobile Applications: A Review[J]. Recent Advances in Sustainable Technologies, 2021: 29-40.

[6] Schmidt O, Gambhir A, Staffell I, et al. Future cost and performance of water electrolysis: An expert elicitation study[J]. International Journal of Hydrogen Energy, 2017, 42(52): 30470-30492.

[7] Rahim A H A, Tijani A S, Kamarudin S K, et al. An overview of polymer electrolyte membrane electrolyzer for hydrogen production: Modeling and mass transport[J]. Journal of Power Sources, 2016, 309: 56-65.

[8] Ni M, Leung M K H, Leung D Y C. Energy and exergy analysis of hydrogen production by a proton exchange membrane (PEM) electrolyzer plant[J]. Energy conversion and management, 2008, 49(10): 2748-

2756.

[9] Bose S, Kuila T, Nguyen T X H, et al. Polymer membranes for high temperature proton exchange membrane fuel cell: recent advances and challenges[J]. Progress in Polymer Science, 2011, 36(6): 813-843.

[10] Shao Y, Yin G, Wang Z, et al. Proton exchange membrane fuel cell from low temperature to high temperature: material challenges[J]. Journal of Power Sources, 2007, 167(2): 235-242.

[11] Nikiforov AV, Garcı´a ALT, Petrushina IM, et al. Preparation and study of IrO2/SiC-Si supported anode catalyst for high temperature PEM steam electrolysers[J]. International Journal of Hydrogen Energy, 2011,36(10):5797-805

[12] Nikiforov A V, Petrushina I M, Christensen E, et al. WC as a non-platinum hydrogen evolution electrocatalyst for high temperature PEM water electrolysers[J]. International journal of hydrogen energy, 2012, 37(24): 18591-18597.

[13] Nikiforov A, Christensen E, Petrushina I, et al. Advanced construction materials for high temperature steam PEM electrolysers[J]. Electrolysis; Linkov, V., Kleperis, J., Eds.; IntechOpen: London, UK, 2012: 61-86.

[14] Hansen MK, Bjerrum N, Christensen E, Jensen JO. PEM water electrolysis at elevated temperatures. Ph.D. thesis. Technical University of Denmark, Department of Chemistry Institut;2012.

[15] Lin H L, Yu T L, Chang W K, et al. Preparation of a low proton resistance PBI/PTFE composite membrane[J]. Journal of power sources, 2007, 164(2): 481-487.

[16] Aili D, Hansen M K, Pan C, et al. Phosphoric acid doped membranes based on Nafion®, PBI and their blends–Membrane preparation, characterization and steam electrolysis testing[J]. international journal of hydrogen energy, 2011, 36(12): 6985-6993.

[17] Hansen M K, Aili D, Christensen E, et al. PEM steam electrolysis at 130 C using a phosphoric acid doped short side chain PFSA membrane[J]. International journal of hydrogen energy, 2012, 37(15): 10992-11000.

[18] Li H, Nakajima H, Inada A, et al. Effect of flow-field pattern and flow configuration on the performance of a polymer-electrolyte-membrane water electrolyzer at high temperature[J]. International Journal of Hydrogen Energy, 2018, 43(18): 8600-8610.

[19] Xu W, Scott K, Basu S. Performance of a high temperature polymer electrolyte membrane water

electrolyser[J]. Journal of Power Sources, 2011, 196(21): 8918-8924.

[20] Garbe S, Futter J, Schmidt T J, et al. Insight into elevated temperature and thin membrane application for high efficiency in polymer electrolyte water electrolysis[J]. Electrochimica Acta, 2021, 377: 138046.

[21] Li H, Inada A, Fujigaya T, et al. Effects of operating conditions on performance of high-temperature polymer electrolyte water electrolyzer[J]. Journal of Power Sources, 2016, 318: 192-199.

[22] Natarajan V, Basu S, Scott K. Effect of treatment temperature on the performance of RuO2 anode electrocatalyst for high temperature proton exchange membrane water electrolysers[J]. International journal of hydrogen energy, 2013, 38(36): 16623-16630.

[23] Tijani A S, Barr D, Rahim A H A. Computational modelling of the flow field of an electrolyzer system using CFD[J]. Energy Procedia, 2015, 79: 195-203.

[24] Ruiz D D H, Sasmito A P, Shamim T. Numerical investigation of the high temperature PEM electrolyzer: effect of flow channel configurations[J]. ECS Transactions, 2013, 58(2): 99.

[25] Zhang Z, Xing X. Simulation and experiment of heat and mass transfer in a proton exchange membrane electrolysis cell[J]. International Journal of Hydrogen Energy, 2020, 45(39): 20184-20193.

[26] Jia Y, Zeng M, Barnoon P, et al. CFD simulation of time-dependent oxygen production in a manifold electrolyzer using a two-phase model[J]. International Communications in Heat and Mass Transfer, 2021, 126: 105446.

[27] Toghyani S, Afshari E, Baniasadi E, et al. Thermal and electrochemical performance assessment of a high temperature PEM electrolyzer[J]. Energy, 2018, 152: 237-246.

[28] Scheepers F, Stähler M, Stähler A, et al. Temperature optimization for improving polymer electrolyte membrane-water electrolysis system efficiency[J]. Applied Energy, 2021, 283: 116270.

[29] Bonanno M, Mueller K, Bensmann B, et al. Evaluation of the Efficiency of an Elevated Temperature Proton Exchange Membrane Water Electrolysis System[J]. Journal of The Electrochemical Society, 2021.

[30] Toghyani S, Baniasadi E, Afshari E. Numerical simulation and exergoeconomic analysis of a high temperature polymer exchange membrane electrolyzer[J]. International Journal of Hydrogen Energy, 2019, 44(60): 31731-31744.

[31] Suwanwarangkul R, Croiset E, Fowler M W, et al. Performance comparison of Fick's, dusty-gas and Stefan–Maxwell models to predict the concentration overpotential of a SOFC anode[J]. Journal of Power

Sources, 2003, 122(1): 9-18.

[32] Kakac S, Pramuanjaroenkij A, Zhou X Y. A review of numerical modeling of solid oxide fuel cells[J]. International journal of hydrogen energy, 2007, 32(7): 761-786.

[33] Xia L, Ni M, He Q, et al. Optimization of gas diffusion layer in high temperature PEMFC with the focuses on thickness and porosity[J]. Applied Energy, 2021, 300: 117357.

[34] Xu H, Chen B, Zhang H, et al. The thermal effect in direct carbon solid oxide fuel cells[J]. Applied Thermal Engineering, 2017, 118: 652-662.

[35] Zhao D, He Q, Yu J, et al. Dynamic behaviour and control strategy of high temperature proton exchange membrane electrolyzer cells (HT-PEMECs) for hydrogen production[J]. International Journal of Hydrogen Energy, 2020, 45(51): 26613-26622.

[36] Luo Y, Shi Y, Li W, et al. Comprehensive modeling of tubular solid oxide electrolysis cell for co-electrolysis of steam and carbon dioxide[J]. Energy, 2014, 70: 420-434.

[37] Torreglosa J P, Jurado F, García P, et al. PEM fuel cell modeling using system identification methods for urban transportation applications[J]. International journal of hydrogen energy, 2011, 36(13): 7628-7640.

[38] Benchouia N E, Derghal A, Mahmah B, et al. An adaptive fuzzy logic controller (AFLC) for PEMFC fuel cell[J]. International Journal of Hydrogen Energy, 2015, 40(39): 13806-13819.

[39] Wu X J, Zhu X J, Cao G Y, et al. Predictive control of SOFC based on a GA-RBF neural network model[J]. Journal of Power Sources, 2008, 179(1): 232-239.

[40] Zhao D, He Q, Wu X, et al. Modeling and optimization of high temperature proton exchange membrane electrolyzer cells[J]. International Journal of Green Energy, 2021.

[41] Carmo M, Fritz D L, Mergel J, et al. A comprehensive review on PEM water electrolysis[J]. International journal of hydrogen energy, 2013, 38(12): 4901-4934.

[42] Falcão D S, Pinto A. A review on PEM electrolyzer modelling: Guidelines for beginners[J]. Journal of Cleaner Production, 2020, 261: 121184.

[43] Elwan H A, Thimmappa R, Mamlouk M, et al. Applications of poly ionic liquids in proton exchange membrane fuel cells: A review[J]. Journal of Power Sources, 2021, 510: 230371.

[44] Coker A K. Appendix C: Physical properties of liquids and gases[J]. Ludwig's Applied Process Design for Chemical and Petrochemical Plants, 2007, 1: 827-862.